

NASA Contractor Report 3212

Aircraft Control by Propeller Cyclic Blades

John DeYoung
Hampton Technical Center
Kentron International, Inc.
Hampton, Virginia

Prepared for
Langley Research Center
under Contract NAS1-13500



National Aeronautics
and Space Administration

**Scientific and Technical
Information Branch**

1979

TABLE OF CONTENTS

	Page No.
SUMMARY	1
INTRODUCTION	1
SYMBOLS	2
SOLUTION FOR CYCLIC-CONTROL PROPELLER CHARACTERISTICS	6
Force and Moment Coefficients in Terms of Azimuth Angle Integrals	6
Cyclic-Control Solutions by Power Series	8
Cyclic function of cosine to m-power	12
Cyclic function for most moment with least extra power, also, with minimum blade-pitching acceleration	14
Denotation of C_T linearity with J by C_T^*	17
Cyclic-Control Solutions in Terms of Bessel Functions	18
Averaged cyclic thrust and power	18
Cyclic pitching and yawing moments	20
Cyclic side and normal forces	21
Estimation of Phase Angle	22
CYCLIC-CONTROL COMPARISONS OF THEORY WITH EXPERIMENT AND EVALUATION OF EXTRA POWER	25
Comparison of Theory with Experiment	25
Cyclic-control moment and change in thrust	26
Cyclic-control force and ideal change in power	28
Extra Power Changes Due to Cyclic Control	30
Vibratory swirl of the slipstream	30
Angled slipstream	32
Pitching airfoil of the propeller blades	33
Vibratory structural damping	34
Total Power Comparisons of Theory with Experiment	34
COUNTERROTATING PROPELLERS AND OTHER CONFIGURATIONS FOR ISOLATING CYCLIC-CONTROL FORCES AND MOMENTS	35
Counterrotating Propeller	36
Cyclic-control analysis	36
Unique cyclic-control characteristics	41
Multipropellers In Line	41

TABLE OF CONTENTS (cont)

	Page No.
RESULTS AND DISCUSSION	43
Guide for Usage of Theory	43
Sinusoidal cycle	43
Steady-state propeller data	44
Arbitrary cyclic function	45
Extra power changes	45
Counterrotating propeller	45
Example Solution and Experimental Comparison	46
Isolated Cyclic-Control Forces and Moments	46
Concurrent control of arbitrary force and moment of a counterrotating propeller	46
Multipropeller	47
Effect of Cyclic Function	47
Propeller Inclination	48
CONCLUSIONS	48
APPENDIX A. - QUASI-STEADY AZIMUTH ANGLE CHANGE DUE TO BLADE CYCLIC PITCHING AT CHORD POSITION ξ_a	49
APPENDIX B. - APPROXIMATE STEADY-STATE PROPELLER THRUST AND POWER COEFFICIENTS AND DERIVATIVES	52
Thrust Coefficient Derivatives	53
Power Coefficient Derivatives	54
REFERENCES	56
FIGURE	57

SUMMARY

A theory is developed for aircraft control obtained from the propeller forces and moments generated by blade angle variation during a blade revolution. The propeller blade is pitched harmonically one cycle per propeller revolution. As a result, the propeller off-set thrust and power produce forces and moments on the axis which provide control for the vehicle. This is termed cyclic-control. Using quasi-steady principles, and a power series representation of an arbitrary function for cyclic-blade angle, theory is developed which leads to exact solutions in terms of derivatives of steady-state thrust and power with respect to blade angle. An alternative solution, when the cyclic-blade angle is sinusoidal, is in terms of Bessel functions. This solution is mathematically valid for cyclic-blade angles to 90 degrees. Steady-state propeller theories and experiments are well documented and available in the literature, and in addition, an approximate method is given in the present report. Needed are the steady-state first and higher order derivatives of thrust and power with respect to steady-state blade angle. An estimate of non-steady azimuth angle change or lag is presented. Correlations of cyclic-control theory predictions are made with experiment.

For vehicle control it is desirable to isolate forces and moments. In this aspect it is shown how the counterrotating propeller is unique. By applying a cyclic-blade angle at the proper azimuth angle on each rotor, a force can be generated in any direction without an accompanying moment on the counterrotating propeller axis, or alternatively, a moment without force. In the hovering mode, cyclic control provides propulsion in any direction to the dual rotor without rotor tilt or moments. Also, when in the propeller mode at the tail of an airship or submarine, this provides isolated or combined control forces and moments with no airship movement. It is shown how three or more single rotation propellers, in line as on a wing, can also isolate control forces and moments by cyclic-control.

INTRODUCTION

In the technical evolution of broadening the high-low speed range capability of aircraft, the propulsive unit, as speed decreases, must increasingly augment both lift and control. Ideally, both would be contained in a single and optimized unit. By making the blades cyclic controllable, the propeller or rotor becomes a propulsive unit in which propulsion, lift, and control are combined, as in some helicopter designs. The term cyclic control refers to harmonically changing the blade angle from $\beta_0 + \gamma$ to $\beta_0 - \gamma$ to $\beta_0 + \gamma$ degrees during each propeller revolution, where γ and the azimuth angle, ψ_0 , at which γ is added, are both controllable. A list of the types of aircraft or the types of operations for cyclic control application would include tilt-wing, tilt-rotor, vectored slipstream by normal or side forces, short take-off and landing, loiter, lifting-crane, airship or submarine, control of slipstream deflection for best cruise, and air-cushion. In some of these applications only a limited number of degrees of freedom is of concern and the term monocyclic propeller has been used. Cyclic-control theory does not become more complicated for more degrees of freedom and can be derived for generalized cyclic control valid for six degrees of freedom.

Cyclic-control experimental data is presented in reference 1 on work done by de Decker. This experimental data is with zero free stream velocity and includes thrust and power, without and with cyclic blade-angle, and side force and pitching moment of the propeller with cyclic blade angle for various blade angle settings. Basic cyclic-control analysis is developed in reference 2. Recent counterrotating-rotor cyclic-control analysis for the helicopter, based on helicopter theory assumptions of low disc loading and small blade and inflow angles, was developed by Drs. Wadia and Fairchild and presented (ref. 3) in a paper. The analysis of reference 2 is partly based on an analogy of cyclic-control, with inclined propeller methods. The theory of a propeller with cyclic change of blade angle is analogous to the theory of the inclined propeller or the propeller in yaw developed in references 4 and 5. The primary difference is that the cyclic-control blade does not sense a dynamic pressure change, whereas, for the inclined propeller, changes in dynamic pressure occur during a cycle. Helicopter theory for cyclic control is simplified to rotors of small solidity and small blade and inflow angles, and is generally inadequate for highly loaded propellers of large solidity. The theory of reference 2 contains the concept that cyclic control on a counterrotating propeller can isolate all control forces and moments. Details of this concept were presented by DeYoung for VLM Corporation to an Army evaluation team USAAMRDL (Ames Research Center), in an unpublished paper, "The Counterrotating Rotor with Cyclic-Control Permits Isolation of Forces and Moments," February 17, 1972, Fort Worth, Texas.

The principal objective of the present study is to present a generalized theory relating cyclic-control forces, moments, power and thrust changes to the steady-state characteristics of the same propeller for arbitrary propeller solidity or disc loading; to derive counterrotating propeller cyclic-control analysis in terms of that of the single propeller solution; and to investigate the effectiveness of propeller or rotor configurations or combinations for isolating cyclic-control forces and moments. The present study starts with a refinement, clarification, and extension of the basic theory developed in reference 2.

SYMBOLS*

B	number of blades	
b	propeller blade chord ($b_{av} = 1.25 \int_{.2}^1 b \, d\rho$)	
C_m	pitching moment coefficient	$\frac{M}{\rho_a n^2 D^5}$

* All forces and moments are acting at propeller hub. See figure 1 for positive directions.

C_N	normal-force coefficient	$\frac{N}{\rho_a n^2 D^4}$
C_n	yawing moment coefficient	$\frac{N_{yaw}}{\rho_a n^2 D^5}$
C_P	power coefficient ($2\pi C_Q$),	$\frac{P}{\rho_a n^3 D^5}$
C_Q	torque coefficient ($C_P/2\pi$),	$\frac{Q}{\rho_a n^2 D^5}$
C_T	thrust coefficient	$\frac{T}{\rho_a n^2 D^4}$
C_Y	side-force coefficient	$\frac{Y}{\rho_a n^2 D^4}$
D	propeller diameter	
F_M	figure of merit (static conditions,	$\sqrt{\frac{2}{\pi}} \frac{C_T^{3/2}}{C_P}$)
J	advance ratio (V/nD)	
J_{0T}	advance ratio at which thrust is zero	
J_{0P}	advance ratio at which power is zero	
$J_n(X)$	Bessel function of the first kind (eq. (44))	
k_P	fractional change of power radial position with blade angle (eq. 57))	
k_T	fractional change of thrust radial position with blade angle (eq. (53))	
n	propeller rotational speed, revolutions per second	
P	power input to propeller	

q	freestream dynamic pressure ($\rho_a v^2/2$)
R	propeller radius
r	radius distance from propeller axis
T	propeller thrust
V	freestream velocity
β	blade angle at $\rho = 3/4$, ($\beta_0 - \epsilon$)
β_0	blade angle at $\rho = 3/4$, measured, from zero lift ($\beta + \epsilon$)
β_1	blade angle at $\rho = 3/4$ for which $\rho \tan\beta(\rho)$ is most constant along radius, measured from zero lift (eq. (54))
γ	maximum cyclic angle, positive at $\psi = \pi$ to give positive pitching moment
ϵ	blade angle between zero lift chord and geometric chord
κ	section $c_{l_\alpha}/2\pi$
ρ	dimensionless radial distance (r/R)
ρ_a	density of air
ρ_m	thrust off-set for pitching ($2 C_m/C_{T_{av}}$)
ρ_p	radius center-of-power position (r_p/R)
ρ_{p0}	ρ_p at blade angle $\beta_0 = \beta_1$ (eq. (57))
ρ_T	radius center-of-thrust position (r_T/R)
ρ_{T0}	ρ_T at blade angle $\beta_0 = \beta_1$ (eq. (53))
σ	effective solidity ($\frac{4B b_{av}}{3\pi D}$)

τ	blade tip correction factor (eq. (66))
ϕ	propeller inflow angle
ψ	azimuth angle, positive clockwise
ψ_0	azimuth angle for maximum cyclic-blade angle (eq. (1))

Subscripts

av	average
o	indicates the steady-state value

Superscripts

','','''	first, second, etc., derivatives with respect to β_0 or β
*	denotes linear with advance ratio from J_{0T}

SOLUTION FOR CYCLIC-CONTROL PROPELLER CHARACTERISTICS

Force and Moment Coefficients in Terms of Azimuth Angle Integrals

For cyclic-control of propeller forces and moments a cyclic variation of blade angle is superimposed on the steady-state blade angle during one revolution of the propeller. When this variation is continually repeated, the thrust and torque will also vary during the cycle and lead to thrust off-set, side forces, and resulting moment changes. The azimuth angle, ψ , is defined as shown in figure 1, also the positive directions of force and moment coefficients are shown. Let

$$\left. \begin{array}{l} \text{for clockwise rotation;} \quad \psi_o = \psi_{ph} + \psi_{ax} + \psi_{con} \\ \text{for counterclockwise rotation;} \quad \psi_o = -\psi_{ph} + \psi_{ax} + \psi_{con} \end{array} \right\} \quad (1)$$

where ψ_o is the azimuth angle at which the blade thrust and torque are minimum, ψ_{ph} is the phase angle that the thrust and torque lag the blade angle, ψ_{ax} is the effective phase angle change due to blade pitching velocity (appendix A), and ψ_{con} is the azimuth angle that can be chosen to govern or control the position of minimum blade thrust. The average thrust and average power coefficients are

$$C_{Tav} = \frac{1}{2\pi} \int_0^{2\pi} C_T(\psi - \psi_o) d\psi \quad (2)$$

$$C_{Pav} = \frac{1}{2\pi} \int_0^{2\pi} C_P(\psi - \psi_o) d\psi \quad (3)$$

where $C_T(\psi - \psi_o)$ and $C_P(\psi - \psi_o)$ represent functional relations of variations with $(\psi - \psi_o)$, and are arbitrary functions.

The hub pitching moment is the product of the thrust and the z component of radial distance of center of thrust, then

$$C_m = - \frac{1}{4\pi} \int_0^{2\pi} \rho_T(\psi - \psi_o) C_T(\psi - \psi_o) \cos \psi d\psi \quad (4)$$

The hub yawing moment is the product of the thrust and the y component of radial distance of center of thrust, then

$$C_n = -\frac{1}{4\pi} \int_0^{2\pi} \rho_T(\Psi-\Psi_0) C_T(\Psi-\Psi_0) \sin \Psi \, d\Psi$$

$$= C_m \tan \Psi_0 \quad (5)$$

where the second equality is obtained by noting that the functional variation of ρ_T and C_T is antisymmetric with $(\Psi-\Psi_0)$ and that

$$\sin \Psi = \cos \Psi_0 \sin(\Psi-\Psi_0) + \sin \Psi_0 \cos(\Psi-\Psi_0)$$

then the first term in this $\sin \Psi$ expansion will be zero in the integration from $\Psi = 0$ to 2π . Similarly, the expansion of $\cos \Psi$ in equation (4) leads to $\cos \Psi_0 \cos(\Psi-\Psi_0)$ and this multiplied by $\tan \Psi_0$ results in $C_n = C_m \tan \Psi_0$.

The side force is the integration of the change of torque normal to the xz-plane, divided by the radial center of torque or power, then

$$C_Y = -\frac{1}{\pi} \int_0^{2\pi} \frac{C_Q(\Psi-\Psi_0)}{\rho_P(\Psi-\Psi_0)} \cos \Psi \, d\Psi = -\frac{1}{2\pi^2} \int_0^{2\pi} \frac{C_P(\Psi-\Psi_0)}{\rho_P(\Psi-\Psi_0)} \cos \Psi \, d\Psi \quad (6)$$

The normal force is the integration of the change of torque normal to the xy-plane, divided by the radial center of power, then

$$C_N = \frac{1}{2\pi^2} \int_0^{2\pi} \frac{C_P(\Psi-\Psi_0)}{\rho_P(\Psi-\Psi_0)} \sin \Psi \, d\Psi = -C_Y \tan \Psi_0 \quad (7)$$

where as in equation (5) the integrand factor of $\sin \Psi$ is antisymmetric.

The thrust off-set for pitching is

$$\rho_m = \frac{z_T}{R} = \frac{M}{R T_{av}} = \frac{2 C_m}{C_{Tav}} \quad (8)$$

The thrust off-set for yawing is

$$\rho_n = \frac{y_T}{R} = \frac{N_{yaw}}{R T_{av}} = \frac{2 C_n}{C_{Tav}} = \rho_m \tan \psi_0 \quad (9)$$

The figure of merit (static conditions) is

$$F_M = \sqrt{\frac{2}{\pi}} \frac{C_T^{3/2}}{C_P} \quad (10)$$

The signs of equations (4) through (7) are for clockwise propeller rotations, however, the final signs and magnitudes of these coefficients will depend on the azimuth angle, ψ_0 . For counterclockwise rotation, equations (4), (5), and (7) remain the same, only the sign of equation (6) for C_Y changes, but the final sign and magnitude will depend on ψ_0 . With the azimuth control angle, ψ_{con} , equal to zero, and ψ_{ax} small, then the counterclockwise rotation has C_m and C_N with the same sign, and C_Y and C_n with opposite sign to that at clockwise rotation, with magnitude the same.

Cyclic-Control Solutions by Power Series

All the functional factors in the integrands of equations (2) through (7) are functions of the blade angle which in steady-state operation would be constant with respect to azimuth angle and equations (4) through (7) would be zero. In cyclic control operation the blade angle is made to vary during the revolution. Let the blade angle be represented by the function

$$\beta(\psi - \psi_0) = \beta_0 + \gamma f(\psi - \psi_0) \quad (11)$$

where γ is the maximum value of the cyclic angle, and $f(\psi - \psi_0)$ represents the variation antisymmetrically of the cyclic angle added to the blade angle during a revolution of the blade (e.g. this function is simply $-\cos(\psi - \psi_0)$ for sinusoidal variation of blade angle). Then the thrust coefficient for a given blade rotational speed and advance ratio, varies as

$$C_T(\psi - \psi_0) = C_T[\beta_0 + \gamma f(\psi - \psi_0)] \quad (12)$$

where the right side denotes that C_T is a function of the term inside the bracket. Equation (12) can be expanded into a power series in terms of γ , thus

$$C_T = C_T \bigg|_{\gamma=0} + \frac{\partial C_T}{\partial \gamma} \bigg|_{\gamma=0} \gamma + \frac{1}{2!} \frac{\partial^2 C_T}{\partial \gamma^2} \bigg|_{\gamma=0} \gamma^2 + \frac{1}{3!} \frac{\partial^3 C_T}{\partial \gamma^3} \bigg|_{\gamma=0} \gamma^3 + \dots \quad (13)$$

The coefficients of the γ series are obtained by taking partial derivatives of equation (12), and letting γ be zero. Then

$$C_T = C_T[\beta_0 + \gamma f(\Psi - \Psi_0)] \stackrel{\gamma=0}{=} C_{T_0}$$

$$\frac{\partial C_T}{\partial \gamma} = \frac{\partial C_T}{\partial [\beta_0 + \gamma f(\Psi - \Psi_0)]} f(\Psi - \Psi_0) \stackrel{\gamma=0}{=} \frac{\partial C_{T_0}}{\partial \beta_0} f(\Psi - \Psi_0)$$

$$\frac{\partial^2 C_T}{\partial \gamma^2} = \frac{\partial^2 C_T}{\partial [\beta_0 + \gamma f(\Psi - \Psi_0)]^2} [f(\Psi - \Psi_0)]^2 \stackrel{\gamma=0}{=} \frac{\partial^2 C_{T_0}}{\partial \beta_0^2} [f(\Psi - \Psi_0)]^2$$

Then equation (12) can be written as

$$\begin{aligned} C_{T(\Psi - \Psi_0)} = C_{T_0} &+ \gamma \frac{\partial C_{T_0}}{\partial \beta_0} f(\Psi - \Psi_0) + \frac{\gamma^2}{2!} \frac{\partial^2 C_{T_0}}{\partial \beta_0^2} [f(\Psi - \Psi_0)]^2 \\ &+ \frac{\gamma^3}{3!} \frac{\partial^3 C_{T_0}}{\partial \beta_0^3} [f(\Psi - \Psi_0)]^3 + \\ &\dots + \frac{\gamma^n}{n!} \frac{\partial^n C_{T_0}}{\partial \beta_0^n} [f(\Psi - \Psi_0)]^n + \dots \end{aligned} \quad (14)$$

when C_{T_0} is the steady-state thrust coefficient ($\gamma = 0$) which is a function of β_0 . Thus in equation (14) the cyclic variation of thrust is expressed simply in terms of steady-state thrust derivatives with respect to blade angle.

A similar expansion gives the power coefficient as

$$\begin{aligned}
 C_p(\psi-\psi_0) &= C_{p_0} + \gamma \frac{\partial C_{p_0}}{\partial \beta_0} f(\psi-\psi_0) + \frac{\gamma^2}{2!} \frac{\partial^2 C_{p_0}}{\partial \beta_0^2} [f(\psi-\psi_0)]^2 + \\
 &\quad \frac{\gamma^3}{3!} \frac{\partial^3 C_{p_0}}{\partial \beta_0^3} [f(\psi-\psi_0)]^3 + \\
 &\quad \dots + \frac{\gamma^n}{n!} \frac{\partial^n C_{p_0}}{\partial \beta_0^n} [f(\psi-\psi_0)]^n + \dots
 \end{aligned} \tag{15}$$

An expansion for the product of radius center-of-thrust and thrust, results in

$$\begin{aligned}
 \rho_T(\psi-\psi_0) C_T(\psi-\psi_0) &= \rho_{T_0} C_{T_0} + \gamma \frac{\partial(\rho_{T_0} C_{T_0})}{\partial \beta_0} f(\psi-\psi_0) + \\
 &\quad \frac{\gamma^2}{2!} \frac{\partial^2(\rho_{T_0} C_{T_0})}{\partial \beta_0^2} [f(\psi-\psi_0)]^2 + \\
 &\quad \dots + \frac{\gamma^n}{n!} \frac{\partial^n(\rho_{T_0} C_{T_0})}{\partial \beta_0^n} [f(\psi-\psi_0)]^n + \dots
 \end{aligned} \tag{16}$$

An expansion of the ratio of power to radius center-of-power gives

$$\begin{aligned}
 \frac{C_p(\psi-\psi_0)}{\rho_p(\psi-\psi_0)} &= \frac{C_{p_0}}{\rho_{p_0}} + \gamma \frac{\partial(\frac{C_{p_0}}{\rho_{p_0}})}{\partial \beta_0} f(\psi-\psi_0) + \frac{\gamma^2}{2!} \frac{\partial^2(\frac{C_{p_0}}{\rho_{p_0}})}{\partial \beta_0^2} [f(\psi-\psi_0)]^2 + \\
 &\quad \dots + \frac{\gamma^n}{n!} \frac{\partial^n(\frac{C_{p_0}}{\rho_{p_0}})}{\partial \beta_0^n} [f(\psi-\psi_0)]^n + \dots
 \end{aligned} \tag{17}$$

Inserting equations (14) through (17) into the corresponding integrands of equations (2) through (7), and noting that $f(\Psi - \Psi_0)$ is antisymmetric so many of the integrals are zero, leads to the solutions

$$C_{Tav} = C_{T0} + \frac{1}{4} I_{P2} C_T'' \gamma^2 + \frac{1}{2} \sum_{\substack{n=4 \\ \text{even}}}^{\infty} \frac{I_{Pn}}{n!} \frac{\partial^n C_T}{\partial \beta_0^n} \gamma^n \quad (18)$$

$$C_{Pav} = C_{P0} + \frac{1}{4} I_{P2} C_P'' \gamma^2 + \frac{1}{2} \sum_{\substack{n=4 \\ \text{even}}}^{\infty} \frac{I_{Pn}}{n!} \frac{\partial^n C_P}{\partial \beta_0^n} \gamma^n \quad (19)$$

$$C_m = -\frac{1}{4} I_{M1} (\rho_T C_T)' \gamma - \frac{1}{4} \sum_{\substack{n=3 \\ \text{odd}}}^{\infty} \frac{I_{Mn}}{n!} \frac{\partial^n (\rho_T C_T)}{\partial \beta_0^n} \gamma^n = C_n \cot \Psi_0 \quad (20)$$

$$C_n = -\frac{1}{4} I_{N1} (\rho_T C_T)' \gamma - \frac{1}{4} \sum_{\substack{n=3 \\ \text{odd}}}^{\infty} \frac{I_{Nn}}{n!} \frac{\partial^n (\rho_T C_T)}{\partial \beta_0^n} \gamma^n = C_m \tan \Psi_0 \quad (21)$$

$$C_Y = -\frac{1}{2\pi} I_{M1} \left(\frac{C_P}{\rho_P} \right)' \gamma - \frac{1}{2\pi} \sum_{\substack{n=3 \\ \text{odd}}}^{\infty} \frac{I_{Mn}}{n!} \frac{\partial^n (C_P/\rho_P)}{\partial \beta_0^n} \gamma^n = -C_N \cot \Psi_0 \quad (22)$$

$$C_N = \frac{1}{2\pi} I_{N1} \left(\frac{C_P}{\rho_P} \right)' \gamma + \frac{1}{2\pi} \sum_{\substack{n=3 \\ \text{odd}}}^{\infty} \frac{I_{Nn}}{n!} \frac{\partial^n (C_P/\rho_P)}{\partial \beta_0^n} \gamma^n = -C_Y \tan \Psi_0 \quad (23)$$

where the I- integrals are defined as

$$I_{Pn} = \frac{1}{\pi} \int_0^{2\pi} [f(\Psi - \Psi_0)]^n d\Psi \quad (24)$$

$$I_{Mn} = \frac{1}{\pi} \int_0^{2\pi} [f(\Psi - \Psi_0)]^n \cos \Psi d\Psi \quad (25)$$

$$I_{Nn} = \frac{1}{\pi} \int_0^{2\pi} [f(\Psi - \Psi_0)]^n \sin \Psi d\Psi = \begin{matrix} n=\text{odd} \\ I_{Mn} \tan \Psi_0 \end{matrix} \quad (26)$$

In equations (18) through (23), the single prime indicates the first partial derivative with respect to β_0 , the double prime indicates the second partial derivative with respect to β_0 , etc.. Equations (18) through (23) are mathematically exact series but remain generalized in that an arbitrary cyclic antisymmetric function of Ψ , represented by $f(\Psi - \Psi_0)$, can be inserted through the I-integrals of equations (24) through (26). The factors of γ^n in the series are derivatives with respect to steady-state blade angle of thrust and power coefficients, or of products or ratios of thrust and power with blade radius center of thrust or power.

Cyclic function of cosine to m-power. - The cyclic function giving a sinusoidal variation and distorted sine variations of blade angle are of immediate interest. Let

$$f(\Psi - \Psi_0) = \cos^m(\Psi - \Psi_0) \quad (27)$$

where m denotes odd integer powers or odd integer roots. The integrals of equations (24) through (26), with equation (27) are

$$I_{Pn} = \frac{1}{\pi} \int_0^{2\pi} \cos^a(\Psi - \Psi_0) d\Psi = \begin{bmatrix} 0 & , a = \text{odd} \\ 4 \frac{\Gamma(\frac{a+3}{2})}{(a+1)\sqrt{\pi} \Gamma(\frac{a+2}{2})} & , a = \text{even} \end{bmatrix} \quad (28)$$

$$I_{Mn} = \frac{1}{\pi} \int_0^{2\pi} \cos^a(\psi - \psi_0) \cos \psi \, d\psi = \begin{cases} \frac{2}{\sqrt{\pi}} \frac{\Gamma(\frac{a+2}{2})}{\Gamma(\frac{a+3}{2})} \cos \psi_0, & a = \text{odd} \\ 0 & , a = \text{even} \end{cases} \quad (29)$$

$$I_{Nn} = \frac{1}{\pi} \int_0^{2\pi} \cos^a(\psi - \psi_0) \sin \psi \, d\psi = \begin{cases} \frac{2}{\sqrt{\pi}} \frac{\Gamma(\frac{a+2}{2})}{\Gamma(\frac{a+3}{2})} \sin \psi_0, & a = \text{odd} \\ 0 & , a = \text{even} \end{cases} \quad (30)$$

where $a=nm$, Γ is the Gamma function, and $a = \text{odd}$, means odd integers or odd fractions, $1/3$, $1/5$, etc.. Using various values of m in equation (27), the effect of the function $f(\psi - \psi_0)$ can be assessed by evaluating the integral factors in equations (24) through (26). With equations (28) and (29), the integral factors for the first two terms in the series, are

m	cyclic-curve description $\cos^m(\psi - \psi_0)$	factors for C_T or C_p eq. (28)		factors for C_m or C_y eq. (29)	
		I_{P2}	I_{P4}	I_{M1}	I_{M3}
1	sinusoidal	1.00	0.75	$1.00 \cos \psi_0$	$0.75 \cos \psi_0$
1/3	bulged-out	1.43	1.16	$1.16 \cos \psi_0$	$1.00 \cos \psi_0$
1/5	bulged-out	1.60	1.36	$1.20 \cos \psi_0$	$1.09 \cos \psi_0$
0	step-function	2.00	2.00	$1.27 \cos \psi_0$	$1.27 \cos \psi_0$
3	reflex	0.63	0.45	$0.75 \cos \psi_0$	$0.49 \cos \psi_0$

The integral factors for C_n or $-C_N$ determined from equation (30), are the same as those for C_m or C_y , except $\sin \psi_0$ replaces $\cos \psi_0$, that is, the $\tan \psi_0$ relation of equations (21) and (23) holds true. As an example, the integral factors inserted into equations (18) through (23), for the sinusoidal curve, $m = 1$, appear as

$$\left.
\begin{aligned}
C_{Tav} - C_{To} &= \frac{1}{4} C_T'' \gamma^2 + \frac{.75}{48} C_T^{IV} \gamma^4 \\
C_{Pav} - C_{Po} &= \frac{1}{4} C_P'' \gamma^2 + \frac{.75}{48} C_P^{IV} \gamma^4 \\
C_m &= -\frac{1}{4} (\rho_T C_T)' \gamma \cos \psi_o - \frac{.75}{24} (\rho_T C_T)''' \gamma^3 \cos \psi_o \\
C_n &= C_m \tan \psi_o \\
C_Y &= -\frac{1}{2\pi} (C_P/\rho_P)' \gamma \cos \psi_o - \frac{.75}{12\pi} (C_P/\rho_P)''' \gamma^3 \cos \psi_o \\
C_N &= -C_Y \tan \psi_o
\end{aligned}
\right\} (31)$$

Examination of the Im_1 factors in the table shows that the step-function cycle generates the largest moments and forces, about 27 percent greater than that of the sinusoidal cycle. However, as shown by the Ip_2 values, the extra power required is double that of the sinusoidal cycle. In the step-function cycle the maximum blade-pitching acceleration becomes infinite.

Cyclic function for most moment with least extra power, also, with minimum blade-pitching acceleration. - For cyclic control an objective is to get the most control of forces and moments with the least extra power requirement. A relationship between moment or force and extra power can readily be obtained from equations (19), (20), and (22). Up to moderate values of the γ -angle, the second integral terms in equations (18) through (23) are negligible, then equation (19) for extra power can be written as

$$C_{P_{av}} - C_{Po} = \frac{C_P''}{4} I_{P2} \gamma^2$$

Solving for γ

$$\gamma = 2 \left(\frac{C_{P_{av}} - C_{Po}}{C_P'' I_{P2}} \right)^{1/2}$$

then with equations (20) and (22)

$$\left. \begin{aligned} C_m &= -\frac{1}{4} I_{M1} (\rho_T C_T)' \gamma = -\frac{1}{2} \left(\frac{I_{M1}^2}{I_{P2}} \right)^{1/2} \left(\frac{C_{p_{av}} - C_{p_0}}{C_p} \right)^{1/2} (\rho_T C_T)' \\ C_Y &= -\frac{1}{2\pi} I_{M1} \left(\frac{C_p}{\rho_p} \right)' \gamma = -\frac{1}{\pi} \left(\frac{I_{M1}^2}{I_{P2}} \right)^{1/2} \left(\frac{C_{p_{av}} - C_{p_0}}{C_p} \right)^{1/2} \left(\frac{C_p}{\rho_p} \right)' \end{aligned} \right\} \quad (32)$$

For large magnitudes of control forces and moments for a given power expenditure, then, as shown in equation (32), the square root of the ratio of I_{M1}^2 to I_{P2} should be as large as possible. With the general cyclic function of equation (27), and equations (28) and (29), values of this ratio for various values of m are as follows:

m	1	1/3	1/5	0	3
$(I_{M1}^2 / I_{P2} \cos^2 \psi_0)^{1/2}$	1	.97	.95	.90	.95

As can be seen, the sinusoidal cyclic function, $m = 1$, gives the best value, however, this square root ratio is not very sensitive with cyclic function since only a ten percent loss is shown for the extreme conditions of a step-function, $m = 0$, cyclic variation.

These m values, other than one, are rather strong distortions and lead to high acceleration points during the cycle. A small variation from sinusoidal that uses the next symmetric harmonic is given by

$$f(\psi - \psi_0) = k \cos(\psi - \psi_0) + (1 - k) \cos 3(\psi - \psi_0) \quad (33)$$

which equals the required unity at $\psi - \psi_0 = 0$. Inserting equation (33) into equations (24) for $n = 2$, and (25) for $n = 1$, results in

$$\left. \begin{aligned} I_{P2} &= k^2 + (1 - k)^2 \\ I_{M1} &= k \cos \psi_0 \end{aligned} \right\} \quad (34)$$

then the square root ratio is

$$\left(\frac{I_{M1}^2}{I_{P2}} \right)^{1/2} = \frac{|\cos \psi_0|}{[1 + (\frac{1-k}{k})^2]^{1/2}} \quad (35)$$

Equation (35) is maximum with $k = 1$, which is, as before, the sinusoidal variation. However, equation (33) will be examined for minimizing angular acceleration peaks. Let $\Psi = \omega t$, where ω is angular velocity, and t is time. Taking the second partial derivative with respect to time of equation (33) gives the angular acceleration of this cyclic function as

$$\frac{\partial^2 f(\Psi - \Psi_0)}{\partial t^2} = \omega^2 [k \cos(\Psi - \Psi_0) + 9(1 - k) \cos 3(\Psi - \Psi_0)] \quad (36)$$

The conditions for minima are obtained by differentiating once again and setting the results equal to zero. Thus

$$\begin{aligned} & \omega^3 [k \sin(\Psi - \Psi_0) + 27(1 - k) \sin 3(\Psi - \Psi_0)] \\ & = \omega^3 [81 - 80k + 108(k - 1) \sin^2(\Psi - \Psi_0)] \sin(\Psi - \Psi_0) = 0 \end{aligned} \quad (37)$$

then

$$\sin^2(\Psi - \Psi_0) = \frac{80k - 81}{108(k-1)} = 0, \quad k = \frac{81}{80} \quad (38)$$

The angular acceleration per angular velocity squared for the sinusoidal cycle is given by $k = 1$ in equation (36). With the k of equation (38), the maximum angular acceleration per angular velocity squared equals 90 percent of the sinusoidal maximum, as shown in the following comparison:

$$\frac{1}{\omega^2} \frac{\partial^2 f(\Psi - \Psi_0)}{\partial t^2}$$

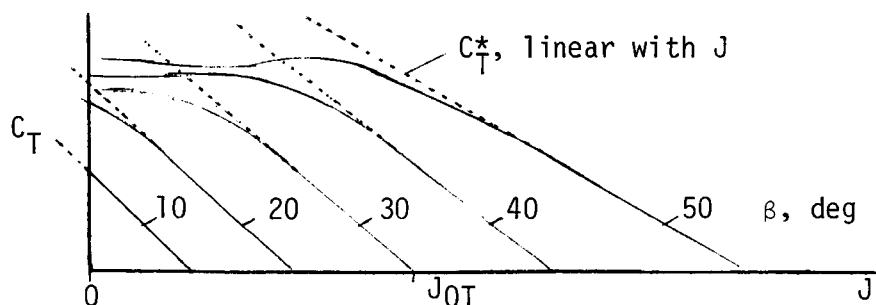
$\Psi - \Psi_0, \text{ deg}$	0	15	30	45	60	75	90
sinusoidal	1.000	.966	.866	.707	.500	.259	0
$k = 81/80$.900	.899	.877	.795	.619	.342	0

Since vibration fatigue depends on the maximum stress, or acceleration, and little on the time rate of change of acceleration, then this $k = 81/80$ function of $f(\Psi - \Psi_0)$, which is little different from sinusoidal, may be optimum. From equation (37), at $\Psi - \Psi_0 = 90$ degrees, the $k = 81/80$ cyclic function has a time rate of change of angular acceleration which is 35 percent larger than that of the sinusoidal cyclic function. From equations (33) through (35), the $k = 81/80$ cyclic function integral factor characteristics are

$$\left. \begin{aligned}
 f(\psi - \psi_0) &= \frac{81}{80} \cos(\psi - \psi_0) - \frac{1}{80} \cos 3(\psi - \psi_0) \\
 I_{P2} &= 1 + \frac{81}{3200} = 1.0253 \\
 I_{M1} &= \frac{81}{80} \cos \psi_0 = 1.0125 \cos \psi_0 \\
 (I_{M1}^2 / I_{P2} \cos^2 \psi_0)^{1/2} &= (1 - 1/6562)^{1/2} \approx 1.000
 \end{aligned} \right\} \quad (39)$$

The blade angle cyclic variation, cyclic forces and moments, and thrust and power, for the $k = 81/80$ cyclic function, are obtained by inserting equation (39) into equations (11) and (18) through (23). Comparing the $k = 81/80$ cyclic function characteristics with those due to a sinusoidal cycle (eq. 31), the $k = 81/80$ cycle has the same moment and force ratio per extra power, 1.25 percent greater moments and forces, 2.53 percent more extra power required, and ten percent less maximum blade angular acceleration which helps delay fatigue.

Denotation of C_T linearity with J by C_T^* . - In equations (18) through (23) the partial derivatives of thrust and power with respect to blade angle are obtained from steady-state experimental propeller charts or from steady-state propeller or rotor theory. Steady-state thrust coefficients tend to become nonlinear with advance ratio as advance ratio becomes small. This nonlinearity is primarily due to the increase in angle of attack on the blade with less increase of lift, as that of a wing approaching stall. In addition, the induced inflow velocity becomes proportionally larger at smaller advance ratios. The blade with cyclic-blade angle sheds plus and minus starting vortices which induce velocities that keep the flow on the blade attached, and the added then lessened induced inflow velocity during a cycle tends to nullify. These non-steady effects thus approximate a thrust linearity with advance ratio as shown below.



With flow remaining attached under cyclic control conditions of no net inflow, there would be no drag rise which leads to power increase. Hence the partial derivatives with respect to blade angle involving power coefficients are taken directly from steady-state experimental data or theory. Taking into account the non-steady effect on thrust coefficient, all the derivatives involving C_T are with C_T linear with J , denoted by C_T^* , for either experimental or

theoretical steady-state propeller or rotor data. Then equations (18) through (23) become

$$C_{T_{av}} - C_{T_0} = \frac{1}{4} I_{P2} C_T^{*''} \gamma^2 + \frac{1}{2} \sum_{\substack{n=4 \\ \text{even}}}^{\infty} \frac{I_{Pn}}{n!} \frac{\partial^n C_T^*}{\partial \beta_0^n} \gamma^n \quad (40)$$

$$C_{P_{av}} - C_{P_0} = \frac{1}{4} I_{P2} C_P^{*''} \gamma^2 + \frac{1}{2} \sum_{\substack{n=4 \\ \text{even}}}^{\infty} \frac{I_{Pn}}{n!} \frac{\partial^n C_P}{\partial \beta_0^n} \gamma^n \quad (41)$$

$$C_m = C_n \cot \psi_0 = -\frac{1}{4} I_{M1} (\rho_T^* C_T^*)' \gamma - \frac{1}{4} \sum_{\substack{n=3 \\ \text{odd}}}^{\infty} \frac{I_{Mn}}{n!} \frac{\partial^n (\rho_T^* C_T^*)}{\partial \beta_0^n} \gamma^n \quad (42)$$

$$C_Y = -C_N \cot \psi_0 = -\frac{1}{2\pi} I_{M1} \left(\frac{C_P}{\rho_P}\right)' \gamma - \frac{1}{2\pi} \sum_{\substack{n=3 \\ \text{odd}}}^{\infty} \frac{I_{Mn}}{n!} \frac{\partial^n (C_P/\rho_P)}{\partial \beta_0^n} \gamma^n \quad (43)$$

where the I integrals are given in equations (24) and (25), and ρ_T^* is the radial position of the center of linear-with-J thrust.

Cyclic-Control Solutions in Terms of Bessel Functions

The integrals of equations (2) through (7) for the sinusoidal cycle can be directly evaluated in terms of Bessel functions since they already contain the integral representations of the Bessel functions. These integrals are characterized by trigonometric functions as arguments of trigonometric functions. For example, from reference 6

$$J_\nu(\gamma) = \frac{(\gamma/2)^\nu}{\Gamma(\nu + \frac{1}{2}) \Gamma(\frac{1}{2})} \int_0^\pi \sin^{2\nu} \psi \cos(\gamma \cos \psi) d\psi, \quad \nu > -\frac{1}{2} \quad (44)$$

Thus the use of Bessel functions provides a closed solution which is valid to large values of the cyclic angle, γ .

Averaged cyclic thrust and power. - The linear with J steady-state thrust coefficient is expressed as a Fourier series in β_0 , thus

$$C_T^* = \sum_{n=0}^{\infty} (a_n \cos n\beta_0 + b_n \sin n\beta_0) \quad (45)$$

The sinusoidal cyclic-blade angle is given by

$$\beta(\Psi - \Psi_0) = \beta_0 - \gamma \cos(\Psi - \Psi_0) \quad (46)$$

Substituting $\beta(\Psi - \Psi_0)$ of equation (46) for β_0 in equation (45), results in

$$C_T^*(\Psi - \Psi_0) = \sum_{n=0}^{\infty} \left\{ (a_n \cos n\beta_0 + b_n \sin n\beta_0) \cos[n\gamma \cos(\Psi - \Psi_0)] - \right. \\ \left. (-a_n \sin n\beta_0 + b_n \cos n\beta_0) \sin[n\gamma \cos(\Psi - \Psi_0)] \right\} \quad (47)$$

A simple means for obtaining the relationship between integrals of trigonometric products and Bessel functions is by use of the following series:

$$\left. \begin{aligned} \cos(\gamma \sin \Psi) &= J_0(\gamma) + 2J_2(\gamma) \cos 2\Psi + 2J_4(\gamma) \cos 4\Psi + \dots \\ \sin(\gamma \sin \Psi) &= 2J_1(\gamma) \sin \Psi + 2J_3(\gamma) \sin 3\Psi + 2J_5(\gamma) \sin 5\Psi + \dots \\ \cos(\gamma \cos \Psi) &= J_0(\gamma) - 2J_2(\gamma) \cos 2\Psi + 2J_4(\gamma) \cos 4\Psi - \dots \\ \sin(\gamma \cos \Psi) &= 2J_1(\gamma) \cos \Psi - 2J_3(\gamma) \cos 3\Psi + 2J_5(\gamma) \cos 5\Psi - \dots \end{aligned} \right\} \quad (48)$$

and noting that

$$\left. \begin{aligned} \int_0^{2\pi} \sin m\Psi \sin n\Psi \, d\Psi &= \int_0^{2\pi} \cos m\Psi \cos n\Psi \, d\Psi = 0, \quad m \neq n \\ \int_0^{2\pi} \sin^2 n\Psi \, d\Psi &= \int_0^{2\pi} \cos^2 n\Psi \, d\Psi = \pi, \quad n \neq 0 \\ \int_0^{2\pi} \sin m\Psi \cos n\Psi \, d\Psi &= 0, \quad \text{all } m \text{ and } n \end{aligned} \right\} \quad (49)$$

where m and n are integers.

The integration of equation (2) with equations (47), (48), and (49), results in the average thrust coefficient, thus

$$C_{T_{av}}^* = \sum_{n=0}^{\infty} (a_n \cos n\beta_0 + b_n \sin n\beta_0) J_0(n\gamma)$$

$$= C_{T_0}^* - \sum_{n=1}^{\infty} (a_n \cos n\beta_0 + b_n \sin n\beta_0) [1 - J_0(n\gamma)] \quad (50)$$

Similarly, for the power coefficient, let

$$C_p = \sum_{n=0}^{\infty} (c_n \cos n\beta_0 + d_n \sin n\beta_0) \quad (51)$$

then

$$C_{p_{av}} = C_{p_0} - \sum_{n=1}^{\infty} (c_n \cos n\beta_0 + d_n \sin n\beta_0) [1 - J_0(n\gamma)] \quad (52)$$

Cyclic pitching and yawing moments. - For integrating equation (4) to obtain C_m , the product of the radial center of thrust and the thrust coefficient can be represented by another Fourier series. However, since ρ_T^* does not vary much with β_0 it can be approximated as follows:

$$\rho_T^* = \rho_{T_0}^* [1 + k_T \sin(\beta_0 - \beta_1)] \quad (53)$$

where

$$\beta_1 = -\frac{3}{4} \left(\frac{\partial \beta}{\partial \rho} \right)_{\rho=3/4} \quad (54)$$

where $\rho_{T_0}^*$ is the radial center of blade, linear-with-J thrust at blade angle $\beta_0 = \beta_1$, and β_1 is the blade angle at $\rho = 3/4$ at which the blade pitch ratio, $p/D = \pi \rho \tan \beta_0(\rho)$ is relatively constant with ρ , that is, $\rho \beta = \text{constant}$, then $\beta = -\rho \partial \beta / \partial \rho$. The constant k_T defines the magnitude of the change of radial position with blade angle. Substituting $\beta_0(\psi - \psi_0)$ of equation (46) for β_0 in equation (53), and factoring this ρ_T^* function to equation (47), the integration of equation (4) results in

$$C_m = \frac{1}{4} \rho_{T_0}^* \cos \psi_0 \sum_{n=0}^{\infty} \left\{ 2(-a_n \sin n\beta_0 + b_n \cos n\beta_0) J_1(n\gamma) + \right.$$

$$k_T (-a_n \sin n\beta_0 + b_n \cos n\beta_0) \sin(\beta_0 - \beta_1) [J_1(n\gamma + \gamma) + J_1(n\gamma - \gamma)] +$$

$$\left. k_T (a_n \cos n\beta_0 + b_n \sin n\beta_0) \cos(\beta_0 - \beta_1) [J_1(n\gamma + \gamma) - J_1(n\gamma - \gamma)] \right\} \quad (55)$$

As an example and a check, let the thrust coefficient be given by $C_T^* = b_1 \sin \beta_0$, then equation (55) reduces to

$$C_m = \frac{1}{4} b_1 \rho_{T_0}^* \cos \psi_0 [2J_1(\gamma) \cos \beta_0 + k_T J_1(2\gamma) \sin(2\beta_0 - \beta_1)] \quad (56)$$

which is the sinusoidal cycle solution for any value of γ . If the Bessel functions are expanded to the third power as

$$J_1(x) = \frac{x}{2} - \frac{x^3}{16}$$

then equation (56) becomes

$$C_m = \frac{1}{4} b_1 \rho_{T_0}^* \cos \psi_0 \left\{ [\cos \beta_0 + k_T \sin(2\beta_0 - \beta_1)] \gamma - \frac{1}{8} [\cos \beta_0 + 4k_T \sin(2\beta_0 - \beta_1)] \gamma^3 \right\}$$

The check of this example solution is that the power series method of equation (42), through $n = 3$, leads to an identical equation. That is, by using $f(\psi - \psi_0) = -\cos(\psi - \psi_0)$, from equation (46), then $IM_1 = -1$, $IM_3 = -3/4$, and $\rho_{T_0}^*$ is the product of equation (53) and $b_1 \sin \beta_0$.

The integration of equation (5) for C_n , is the same as for C_m except a factor $\sin \psi_0$ replaces $\cos \psi_0$. Then as before

$$C_n = C_m \tan \psi_0 \quad (5)$$

Cyclic side and normal forces. - For integrating equation (6) to obtain C_Y , an approximate expression for the radial center of torque or power, ρ_p , can be made as developed for ρ_T in equation (53). Let

$$\frac{1}{\rho_p} = \frac{1}{\rho_{p_0}} [1 + k_p \sin(\beta_0 - \beta_1)] \quad (57)$$

where ρ_{p_0} is the radial center of power at the same conditions cited under equation (53), and the constant k_p defines the magnitude of the change of radial position with blade angle. With the sinusoidal cyclic-blade angle of equation (46) inserted into equation (51), the cyclic power variation is

$$C_p(\psi - \psi_0) = \sum_{n=0}^{\infty} \left\{ (c_n \cos n\beta_0 + d_n \sin n\beta_0) \cos[n\gamma \cos(\psi - \psi_0)] + (c_n \sin n\beta_0 - d_n \cos n\beta_0) \sin[n\gamma \cos(\psi - \psi_0)] \right\} \quad (58)$$

Substituting $\beta_0(\psi - \psi_0)$ of equation (46) for β_0 in equation (57), and factoring this $1/\rho_p$ function to equation (58), the integration of equation (6) gives

$$C_Y = \frac{\cos \psi_0}{2\pi \rho_p} \sum_{n=0}^{\infty} \left\{ 2(-c_n \sin n\beta_0 + d_n \cos n\beta_0) J_1(n\gamma) + \right. \\ \left. k_p(-c_n \sin n\beta_0 + d_n \cos n\beta_0) \sin(\beta_0 - \beta_1) [J_1(n\gamma + \gamma) + J_1(n\gamma - \gamma)] + \right. \\ \left. k_p(c_n \cos n\beta_0 + d_n \sin n\beta_0) \cos(\beta_0 - \beta_1) [J_1(n\gamma + \gamma) - J_1(n\gamma - \gamma)] \right\} \quad (59)$$

which, except for notation changes, is the same equation as that for C_m in equation (55).

The integration of equation (7) for C_N , is the same as for C_Y except a factor $\sin \psi_0$ replaces $\cos \psi_0$. Then as before

$$C_N = -C_Y \tan \psi_0 \quad (7)$$

For the same reasons as those given in the section, Denotation of C_T linearity with J by C_T^* , the steady-state thrust coefficient in equation (45) is the C_T that varies linearly with advance ratio J . However, the steady-state power coefficient C_p in equation (51) can have a nonlinear variation with advance ratio.

Estimation of Phase Angle

With cyclic control the blade has a variation of angle of attack during a cycle or blade revolution and the blade lift builds up and decreases in a harmonic fashion and appears as unsteady motion. As angle of attack increases, circulation increases, and a starting vortex is shed which induces a downwash and changes the build-up of circulation. In general, unsteady motion causes the lift cycle to be out of phase with the angle of attack cycle. An approximation for the propeller phase angle can be obtained from an analogous wing unsteady solution. In reference 4 an equation is presented which gives the phase angle lag of forces and moments due to harmonic pitching of a wing about the quarter-chord line, given by

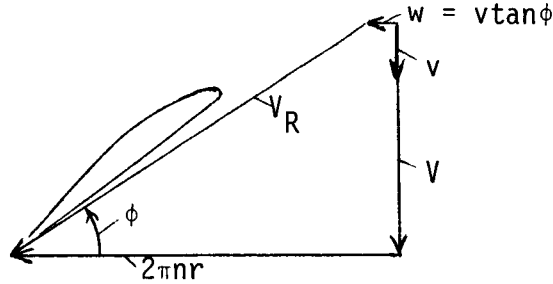
$$\psi_{ph} = 0.825 \tan^{-1} 2.027k \quad (60)$$

$$k = \frac{b \omega_{pitch}}{2V_{eff}} \quad (61)$$

where the phase angle is almost independent of aspect ratio. In equation (61) k is the reduced frequency, b is the section chord, and ω_{pitch} is pitching angular velocity. For the cyclic-control blade the pitching is at the blade rotation, then

$$\omega_{\text{pitch}} = 2\pi n \quad (62)$$

The effective velocity the blade senses is V_R as shown below, in which slipstream rotation is taken into account.



Then for the single propeller or rotor

$$V_R = [(2\pi nr - v \tan \phi)^2 + (V + v)^2]^{1/2}, \quad \tan \phi = \frac{V + v}{2\pi nr - v \tan \phi} \quad (63)$$

Solving the second equation for $v \tan \phi$, results in

$$v \tan \phi = \pi nr - [(\pi nr)^2 - (V + v)v]^{1/2}$$

then with $J = V/nD$, $\rho = r/R$, V_R in nondimensional form becomes

$$\frac{V_R}{nD} = \left\{ \frac{1}{2} \pi^2 \rho^2 + J(J + \frac{v}{nD}) + \pi \rho \left[\frac{1}{4} \pi^2 \rho^2 - (J + \frac{v}{nD}) \frac{v}{nD} \right]^{1/2} \right\}^{1/2} \quad (64)$$

From momentum theory

$$\frac{v}{nD} = \frac{1}{2} \left[\left(J^2 + \frac{8}{\pi \tau^2} C_T \right)^{1/2} - J \right] \quad (65)$$

where τ is the tip-loss correction, for which approximations developed by L. Prandtl are given in references 7 and 8. A modification of Prandtl's correction is

$$\tau = 1 - \frac{\sin \phi_0}{B} = 1 - \frac{J + \frac{v}{nD}}{B \frac{V_R}{nD}} \quad (66)$$

which can be evaluated by iteration with equations (65) and (64) for $\rho = 3/4$. Equation (65) inserted into (64), with $\rho = 3/4$, for a single rotor, is

$$\left(\frac{4}{3\pi} \frac{V_R}{nD}\right)_{\text{single}} = \left\{ \frac{1}{2} + \frac{1}{2} \left(1 - \frac{128C_{T_0}}{9\pi^3 \tau^2}\right)^{1/2} + \frac{8J}{9\pi^2} \left[J + \left(J^2 + \frac{8C_{T_0}}{\pi\tau^2}\right)^{1/2}\right] \right\}^{1/2} \quad (67)$$

For counter-rotating rotors, which are near each other along the axis, w is approximately zero. Letting the $v \tan \phi$ terms be zero in equation (63), then

$$\tan \phi = \frac{V + v}{2\pi n r} \quad (68)$$

and V_R with $\rho = 3/4$, using equation (65), is

$$\left(\frac{4}{3\pi} \frac{V_R}{nD}\right)_{\text{counter}} = \left\{ 1 + \frac{32C_{T_0}}{9\pi^3 \tau^2} + \frac{8}{9\pi^2} J \left[J + \left(J^2 + \frac{8C_{T_0}}{\pi\tau^2} \right)^{1/2} \right] \right\}^{1/2} \quad (69)$$

where C_{T_0} is the thrust coefficient of one of the two counter-rotating rotors, or one-half of the C_{T_0} of the total propeller. From equations (61) and (62), the reduced frequency is

$$k = \frac{\pi n b}{V_R} = \frac{\frac{4}{3} \frac{b_{3/4}}{D}}{\frac{4}{3\pi} \frac{V_R}{nD}} = \frac{\pi \frac{b_{3/4}}{b_{av}} \frac{\sigma}{B}}{\frac{4}{3\pi} \frac{V_R}{nD}} \quad (70)$$

where B is the number of blades on each rotor, and σ is the effective solidity of each rotor, defined in the relation

$$\sigma = \frac{4B}{3\pi} \frac{b_{av}}{D} \quad (71)$$

The phase angle from equation (60), with equation (70), is

$$\psi_{ph} = 0.825 \tan^{-1} \frac{6.368 \frac{b_{3/4}}{b_{av}} \frac{\sigma}{B}}{\frac{4}{3\pi} \frac{V_R}{nD}} \quad (72)$$

where the denominator in the arc tangent function is given in equation (67) for the single rotor, and given in equation (69) for each of the counterrotating rotors. The phase angle is the azimuth angle lag which thrust and torque lag the blade angle variation. Thus, maximum thrust occurs an angle ψ_{ph} after maximum blade angle. The basic azimuth angle, ψ_0 , which governs the components of the cyclic-control forces and moments, is given in equation (1). By using equation (1), for counter-rotating rotors, the clockwise rotation rotor has,

$\psi_o = \psi_{ph} + \psi_{ax} + \psi_{con}$, while the counterclockwise rotation rotor has,
 $\psi_o = -\psi_{ph} + \psi_{ax} + \psi_{con}$. The ψ_o angle can be made the same for the counter-rotating propeller by using a different control angle, ψ_{con} , on each rotor. Since the variation of V_R/nD with thrust coefficient is small, the phase angle will change little with thrust. The V_R velocity increases moderately with advance ratio, then the phase angle will decrease as J increases. At static conditions, $J = 0$, the phase angle will slightly increase with thrust increase for the single rotor, and decrease with thrust increase for each of the counterrotating rotors.

This derivation of phase angle is based on the wing, or blade, with non-separated flow. If the cyclic-blade pitching is made about the stall c_{ℓ} of the blade, then it is operating in a $c_{\ell} \sim \alpha$ hysteresis loop in which the air adds energy to the blade. Then the phase angle is approximately given by a negative value of equation (72) when $k < 0.3$, as shown by an experimental example in reference 9.

CYCLIC-CONTROL COMPARISONS OF THEORY WITH EXPERIMENT AND EVALUATION OF EXTRA POWER

The cyclic-control theoretical results of equations (40) through (43), and (50), (52), (55), and (59), are based on knowing the steady-state values of thrust, thrust linear with advance ratio, and power coefficients. Here steady state refers to the condition that maximum cyclic-blade angle is zero, $\gamma = 0$, and C_T , C_T^* , and C_p versus J for the given propeller are obtained from available propeller chart data, or from a favored propeller theory. An approximate steady-state prediction method from reference 4, for estimating thrust and power coefficients and their derivatives, is further developed and presented in appendix B. The experimental study reported in reference 1 contains propeller cyclic-control experimental data and steady-state data for $J = 0$. The objectives are to show an example usage of the theory, correlate with experiment, and develop relations for extra power due to cyclic control. The cyclic-control power is the ideal power plus extra power where extra is that power other than ideal traceable to the varying cyclic-blade angle.

Comparison of Theory with Experiment

When the cyclic-blade angle γ is small, then the terms γ^n for $n > 2$ are negligible. Then equations (40) through (43) for the sinusoidal cycle, $f(\psi - \psi_o) = \cos(\psi - \psi_o)$, simplify to

$$\frac{C_{T_{av}} - C_T}{\gamma^2 C_T} = \frac{1}{4} \frac{C_T^{*''}}{C_T} \quad (73)$$

$$\left(\frac{C_{p_{av}} - C_p}{\gamma^2 C_p} \right)_{\text{ideal}} = \frac{1}{4} \frac{C_p''}{C_p} \quad (74)$$

$$\frac{C_{m_Y}}{C_T} = \frac{C_{n_Y}}{C_T} \cot \psi_0 = -\frac{1}{4} \left(\rho_T^* \frac{C_T^*'}{C_T} + \frac{C_T^*}{C_T} \rho_T^{*'} \right) \cos \psi_0 \quad (75)$$

$$\frac{C_{Y_P}}{C_P} = -\frac{C_{N_Y}}{C_P} \cot \psi_0 = -\frac{1}{2\pi} \left[\frac{1}{\rho_P} \frac{C_P'}{C_P} + \left(\frac{1}{\rho_P} \right)' \right] \cos \psi_0 \quad (76)$$

In the experiment, all the quantities on the left side of equations (73) through (76) are measured at the condition of $J = 0$. Also the steady state, that is, $\gamma = 0$, thrust and power coefficient are measured at $J = 0$. In this section the experimental steady-state values of C_T and C_P are used to determine the thrust and power derivatives. Using these derivatives, the theoretical values of cyclic-control forces, moments, change in thrust, and change in power, are determined from equations (73) through (76), and compared with measured values.

Cyclic-control moment and change in thrust. - The experiment values of C_T were measured at $J = 0$. For the cyclic-control theory a relation between C_T and C_T^* is that in equation (B18) of appendix B. Since both $\partial C_T / \partial J$ and J_{0T} in equation (B18) are functions of β_0 , then the C_T^* derivatives are obtainable. An approximate $C_T \sim C_T^*$ relation is given in equation (B10), and C_T^* derivatives in terms of C_T derivatives are given in equations (B19) through (B22). These derivatives are applicable for the $J = 0$, C_T measurements.

The geometric characteristics of the propeller used in the test are as follows:

$$\left. \begin{aligned} B = 3, \frac{b_{av}}{D} &= .1178, \sigma = .15, \beta_0 = \beta + \epsilon, \epsilon = 2^\circ \\ J = 0, \kappa &= .9, \delta_0 = .015, \beta_1 = 17^\circ, d_0 = .025 \\ e_T &= .343, e_P = .634, J_{0T} = 2.246 \tan \beta_0 \end{aligned} \right\} \quad (77)$$

where σ , β_1 , d_0 , e_T , e_P , and J_{0T} are determined from equations (71), (54), (B9), (B3), (B4), and (B5), respectively. Curve fitting a function for the experimental static steady-state thrust data, leads to the relationship

$$C_T = .296 \sin(2\beta + 3^\circ) \quad (78)$$

then the derivatives with respect to β are

$$\frac{C_T'}{C_T} = \frac{2}{\tan(2\beta + 3^\circ)} \quad (79)$$

$$\frac{C_T''}{C_T} = -4 \quad (80)$$

An approximation of the ρ_T^* function is given in equation (53). The derivative with respect to β_0 is

$$\rho_T^{*'} = \rho_{T0}^* k_T \cos(\beta_0 - \beta_1) \quad (81)$$

For typical propellers

$$\rho_{T0}^* \approx \frac{2}{3}, \quad k_T \approx \frac{1}{7 \sin(\beta_1 + 5^\circ)} \quad (82)$$

With the values of equation (77), and with equations (53), (81), and (82), equations (73) and (75) become

$$\frac{\Delta C_T}{\gamma^2 C_T} = \frac{C_{Tav} - C_T}{\gamma^2 C_T} = \frac{1}{4} \frac{C_T^{*''}}{C_T} \quad (83)$$

$$\frac{C_m}{C_T \cos \psi_0} = -\frac{1}{6} \left\{ [1 + .381 \sin(\beta_0 - 17^\circ)] \frac{C_T^{*'}}{C_T} + .381 E^{1/2} \cos(\beta_0 - 17^\circ) \right\} \quad (84)$$

where $C_T^{*'}/C_T$, and $C_T^{*''}/C_T$, from equations (B19) and (B20), with equations (79) and (80), are

$$\frac{C_T^{*'}}{C_T} = \left[\frac{2}{\tan(2\beta + 3^\circ)} + \frac{E_T'}{E_T} \right] E_T^{1/2} \quad (85)$$

$$\frac{C_T^*}{C_T} = \left[-4 + \frac{2}{\tan(2\beta + 3)} \frac{E_T'}{E_T} - \frac{1}{4} \left(\frac{E_T'}{E_T} \right)^2 + \frac{1}{2} \frac{E_T''}{E_T} \right] E_T^{1/2} \quad (86)$$

where from equations (B12), (B21), and (B22), E_T and derivatives are

$$E_T = 1 + .7353 (1 + .375 \sin 2\beta_0)^2 \quad (87)$$

$$E_T' = 1.1030 (\cos 2\beta_0 + .1875 \sin 4\beta_0) \quad (88)$$

$$E_T'' = 2.2059 (.375 \cos 4\beta_0 - \sin 2\beta_0) \quad (89)$$

The values determined from equations (78), (83), and (84), are compared with experiment for given values of blade angle, as follows:

β deg	β_0 deg	C_T		$\Delta C_T / \gamma^2 C_T$	$-C_{m_Y} / C_T \cos \psi_0$	
		eq. (78)	experiment	eq. (83)	eq. (84)	experiment
8	10	.0963	.092	-.213	1.438	1.33
10	12	.1156	.112	-.493	1.222	1.22
12	14	.1344	.134	-.708	1.066	1.03
14	16	.1525	.153	-.808	.946	.93
16	18	.1698	.172	-1.024	.849	.85
18	20	.1863	.188	-1.168	.767	.78
20	22	.2019	.203	-1.256	.696	.72
22	24	.2164	.216	-1.350	.632	.66

As shown in these results, the C_T of equation (78) duplicates C_T of the experiment quite accurately. For γ not large, the theoretical thrust loss is negligible at small β , but with greater loss at large blade angles. In the experiment the thrust has a slight loss only at the higher β angle. The pitching moment coefficients correlate within the accuracy of the measurements.

Cyclic-control force and ideal change in power. - Development of an analytical function for a curve fitting the experimental static steady-state propeller power data, leads to the relationship

$$C_p = .292 \frac{\tan^2 (\beta + 11^\circ)}{\cos^3 \beta} \quad (90)$$

then the derivatives with respect to β are

$$\frac{C_p'}{C_p} = \frac{2}{\tan (\beta + 11^\circ)} + 2 \tan (\beta + 11^\circ) + 3 \tan \beta \quad (91)$$

$$\frac{C_p''}{C_p} = \frac{2}{\tan^2 (\beta + 11^\circ)} + 11 + 6 \tan^2 (\beta + 11^\circ) - 6 \tan^2 \beta + 6 \frac{C_p'}{C_p} \tan \beta \quad (92)$$

where $\beta = \beta_0 - 2^\circ$.

The function $1/\rho_p$ is needed in equation (76). An approximation of $1/\rho_p$ is given in equation (57). The derivative with respect to β_0 is

$$\left(\frac{1}{\rho_p}\right)' = \frac{k_p}{\rho_{p_0}} \cos (\beta_0 - \beta_1) \quad (93)$$

For typical propellers

$$\rho_{p_0} \cong \frac{8}{11}, \quad k_p \cong -\frac{1}{11 \sin (\beta_1 + 5^\circ)} \quad (94)$$

With the propeller values listed in equation (77), and with equations (57), (93), and (94), equations (74) and (76) become

$$\frac{\Delta C_{p \text{ ideal}}}{\gamma^2 C_p} = \left(\frac{C_{p \text{ av}} - C_p}{\gamma^2 C_p} \right)_{\text{ideal}} = \frac{1}{4} \frac{C_p''}{C_p} \quad (95)$$

$$\frac{C_{Y \gamma}}{C_p \cos \psi_0} = -.2188 \left\{ [1 - .243 \sin (\beta_0 - 17^\circ)] \frac{C_p'}{C_p} - .243 \cos (\beta_0 - 17^\circ) \right\} \quad (96)$$

where C_p , C_p' , and C_p'' are given in equations (90), (91), and (92), respectively.

The values determined from equations (90), (95), and (96) are compared with experiment for given values of blade angle, as follows:

β deg	β_0 deg	C_p		$\Delta C_p / \gamma^2 C_p$		$-C\gamma_\gamma / C_p \cos \psi_0$	
		eq. (90)	experi- ment	eq. (95)	experi- ment	eq. (96)	experi- ment
8	10	.0357	.036	8.574	16.1	1.505	1.17
10	12	.0451	.046	8.039	13.3	1.400	1.28
12	14	.0563	.057	7.704	11.6	1.320	1.35
14	16	.0695	.070	7.515	9.8	1.259	1.44
16	18	.0853	.084	7.439	10.7	1.211	1.15
18	20	.1043	.102	7.454	9.7	1.176	1.00
20	22	.1270	.127	7.547	10.5	1.151	1.21
22	24	.1546	.155	7.711	8.7	1.134	1.00

It can be seen that the C_p of equation (90) duplicates C_p of the experiment quite accurately. The experimental data of side force coefficient is somewhat erratic, however, the predictions show a correlation with experiment of magnitude and that $C\gamma_\gamma / C_p$ decreases with increasing β . The predicted change in power due to cyclic control is the ideal change in power, analogous to induced drag. The obviously higher measured change in power includes the ideal power change, plus extra or additional power expenditures. This extra power includes power required effects peculiar to cycle control but nonexistent in steady-state operation. Extra power characteristics are investigated in a subsequent section.

Extra Power Changes Due to Cyclic Control

Extra power changes include energies due to a vibratory swirl of the slipstream, angled slipstream, pitching airfoil of the propeller blades, and vibratory structural damping. An estimate of these extra power expenditures can be made without excessive complication.

Vibratory swirl of the slipstream. - For the steady-state propeller, part of the power is used to swirl or rotate the slipstream, and this part equals the time rate of change of the kinetic energy of the slipstream rotation. Similarly, the cyclic-control propeller swirls the slipstream in one direction, then reverses the swirl during the other half of the cycle, or results in a vibratory frequency equal to the propeller revolutions per second. Thus the cyclic-control propeller leaves vibratory swirl kinetic energy in the slipstream which the steady-state propeller does not. This kinetic energy per unit length of the slipstream is

$$\frac{K.E.}{\ell} = \frac{1}{2} \frac{I}{\ell} \dot{\psi}_{sw}^2$$

where the moment of inertia per unit length of a circular column of air is given by

$$\frac{I}{\ell} = \frac{\text{mass}}{\ell} \frac{R^2}{2} = \frac{\pi}{2} \rho_a R^4$$

and $\dot{\Psi}_{sw}$ is the swirl angular velocity. With cyclic control, $\Psi_{sw} = \Psi_{sw0} \cos \omega t$, then $\dot{\Psi}_{sw} = -\Psi_{sw0} \omega \sin \omega t$. The kinetic energy in a complete revolution is the integration of $\dot{\Psi}_{sw}^2$, or

$$\frac{\text{K.E.}}{\ell} = \frac{1}{2} \frac{I}{\ell} \int_0^{2\pi} \Psi_{sw0}^2 \omega^2 \sin^2 \Psi d\Psi = \frac{\pi}{2} \frac{I}{\ell} \omega^2 \Psi_{sw0}^2$$

where Ψ_{sw0} is the maximum swirl angle due to γ . The swirl power is the kinetic energy per unit length times the velocity increase through the propeller disc, then with the I/ℓ expression and since $\omega = 2\pi n$

$$P_{sw} = \rho_a \pi^4 n^2 R^4 \Psi_{sw0}^2 v$$

or

$$C_{P_{sw}} = \frac{\pi^4}{16} \Psi_{sw0}^2 \frac{v}{nD} \quad (97)$$

where v is the average velocity increase through the propeller disc. From simple momentum theory, for example, reference 7, p. 188, the inflow velocity in terms of C_p is obtained by the solution of a cubic equation, then

$$\begin{aligned} \frac{v}{nD} = -\frac{2}{3} J + \left[\frac{J^3}{27} + \frac{C_p}{\pi} + \left(\frac{2J^3 C_p}{27\pi} + \frac{C_p^2}{\pi^2} \right)^{1/2} \right]^{1/3} + \left[\frac{J^3}{27} + \frac{C_p}{\pi} - \left(\frac{2J^3 C_p}{27\pi} + \frac{C_p^2}{\pi^2} \right)^{1/2} \right]^{1/3} \\ J = 0 \quad \frac{C_p^2}{\pi^2} \quad \frac{2C_p}{\pi} \end{aligned} \quad (98)$$

Similarly, the maximum swirl angle can be estimated from momentum theory. Then

$$\left(1 - \frac{1}{2} \Psi_{sw0}\right) \left(\frac{1}{2} \Psi_{sw0}\right) = \frac{2C_T}{\pi \rho^2} = \frac{2/3 \cdot 9C_T}{2\pi}$$

where here $C_T = C_T^*(\beta_0 + \gamma) - C_T^*(\beta_0)$. This C_T can be approximated by using equation (B1), then

$$\Psi_{sw0} \approx \frac{9e_T}{\pi} (2.2 \cos \beta_0 + J \sin \beta_0) \gamma \quad (99)$$

With equation (99), the power expended for vibratory swirling the slipstream, equation (97), becomes

$$\frac{C_{p_{sw}}}{\gamma C_p} = \frac{1}{C_p} \left(\frac{9e_T}{4\pi} \right)^2 (2.2 \cos \beta_0 + J \sin \beta_0)^2 \frac{v}{nD} \quad (100)$$

where v/nD is given in equation (98), and e_T in equation (B3). For $J = 0$, equation (100) simplifies to

$$\frac{C_{p_{sw}}}{\gamma C_p} = 2.136 \frac{e_T^2}{C_p^{2/3}} \cos^2 \beta_0 \quad (101)$$

Angled slipstream. - When the cyclic-blade angle is applied for pitching, a side force is developed. The reaction to this side force produces a slipstream angle opposing the side force. This slipstream angle, represented by ϵ_Y , equals

$$\epsilon_Y = \tan^{-1} \frac{C_Y}{C_T} = \frac{C_Y}{C_T}$$

or for an arbitrary angle of ψ_0 , and using equation (7)

$$\epsilon_Y = \frac{1}{C_T} (C_Y \cos \psi_0 - C_N \sin \psi_0) = \frac{C_Y}{C_T \cos \psi_0} \quad (102)$$

Because of the conservation of momentum, due to slipstream constriction the slipstream velocity increases approximately as

$$V_j(\epsilon_Y) \approx \frac{V_{j0}}{\cos \epsilon_Y}, \quad \text{where } V_{j0} = V + v$$

From momentum theory

$$P = 2\pi R^2 \rho_a V_{j0}^2 (V_{j0} - V)$$

$$P_c = 2\pi R^2 \rho_a \frac{V_{j0}^2}{\cos^3 \epsilon_Y} (V_{j0} - V \cos \epsilon_Y)$$

The ratio gives

$$\frac{C_{p_\epsilon}}{C_p} = \frac{1}{\cos^3 \epsilon_\gamma} \left(\frac{V_{j0} - V \cos \epsilon_\gamma}{V_{j0} - V} \right) = \frac{1}{\cos^3 \epsilon_\gamma} \left[1 - \frac{(1 - \cos \epsilon_\gamma)J}{\frac{v}{nD}} \right]$$

with equation (102)

$$\frac{1}{\cos^3 \epsilon_\gamma} = (1 + \tan^2 \epsilon_\gamma)^{3/2} \cong 1 + \frac{3}{2} \left(\frac{C_\gamma}{C_T \cos \psi_0} \right)^2$$

$$1 - \cos \epsilon_\gamma = 2 \sin^2 \frac{\epsilon_\gamma}{2} \cong \frac{1}{2} \left(\frac{C_\gamma}{C_T \cos \psi_0} \right)^2$$

With these relations, the change in power coefficient, $C_{p_\epsilon} - C_p$, is the angled slipstream power coefficient, given by

$$\frac{C_{p_{ang}}}{\gamma^2 C_p} \cong \frac{3}{2} \left(\frac{C_{\gamma\gamma}}{C_T \cos \psi_0} \right)^2 \left(1 - \frac{J}{3 \frac{v}{nD}} \right) \quad (103)$$

where v/nD is given in equation (98). Equation (103) is an estimate of the fractional power increase due to the angling of the slipstream due to cyclic angle γ . It can be noted that for the counterrotating propeller if one rotor operates at ψ_0 , and the other rotor at $\pi - \psi_0$, then by equation (82) the net C_γ is zero. Thus from equation (103), $C_{p_{ang}}$ is zero, and from equation (102), ϵ_γ is zero.

Pitching airfoil of the propeller blades. - Energy is imparted to the airstream due to forced pitching of an airfoil. An estimate of this energy per unit time is given in reference 9, page 169. For pitching airfoil blades, the power due to blade pitching is

$$P_p = \frac{\pi}{16} \rho_a B R b^4 \omega^3 \gamma^2$$

where in coefficient form is

$$\frac{C_{p_p}}{\gamma^2} = \frac{\pi}{4} B \left(\frac{b_{av}}{D} \right)^4 \quad (104)$$

where b_{av}/D is related with effective solidity in equation (71).

Vibratory structural damping. - The power absorbed in structural damping in a propeller is small, but can be larger for the less rigid helicopter blade. Structural damping is discussed in reference 9, page 227. The power expenditure for damping, due to pitching, is approximated as

$$P_{\text{damp}} = \frac{BI_{\alpha} g_{\alpha} \omega_{\alpha}^2}{2\omega} \int_0^{2\pi} \left(\frac{\partial \beta}{\partial t}\right)^2 d\psi = \frac{\pi}{2} BI_{\alpha} g_{\alpha} \omega_{\alpha}^2 \omega \gamma^2$$

where I_{α} is the moment of inertia of the blade, ω_{α} is the natural angular frequency of the blade, and g_{α} is the damping coefficient which is a fraction of the elastic coefficients. Empirically, g_{α} is found to depend on the amplitude of motion, and power could probably be better represented as proportional to γ^3 . The moment of inertia of a blade is approximately

$$I_{\alpha} \cong \frac{\pi}{128} \rho_b t(1+t^2)b^4 D$$

where ρ_b is the blade density, t is maximum thickness to chord ratio, b is blade chord, and D is propeller diameter. Then the structural damping power coefficient is

$$\frac{C_{p_{\text{stru}}}}{\gamma^2} = \frac{\pi^5}{32} B \left(\frac{b_{av}}{D}\right)^4 t(1+t^2) \left(\frac{\omega_{\alpha}}{\omega}\right)^2 \frac{\rho_b}{\rho_a} g_{\alpha} \quad (105)$$

where ρ_b/ρ_a is the ratio of blade density to air density.

Total Power Comparisons of Theory with Experiment

The total power is the sum of the ideal and the four extra power requirements of the cyclic-control propeller or rotor. The test propeller characteristics are listed in equation (77). In addition, estimates of the blade density ratio, natural angular frequency of the blade, blade damping coefficient, and thickness ratio are

$$\left. \begin{array}{l} \left(\frac{\omega_{\alpha}}{\omega}\right)^2 \cong 4000 \\ \frac{\rho_b}{\rho_a} \cong 2200 \\ g_{\alpha} \cong 10^{-5} \\ t = .09 \end{array} \right\} \quad (106)$$

which approximate that of an aluminum blade with tip speed of about .8 Mach number. The damping coefficient of a wing is typically of the order $g_\alpha = 10^{-3}$ to 10^{-2} . The propeller blade is much more rigid than a wing and g_α is assumed to be one percent that of a wing. For these propeller values, the power coefficient changes due to cyclic-control are compared in the following table:

$$\Delta C_p / \gamma^2 C_p$$

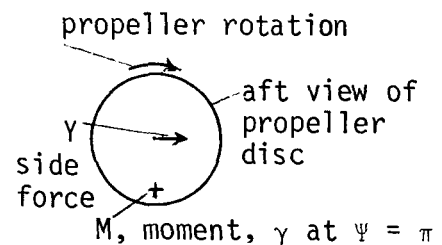
β deg	ideal eq. (95)	swirl eq. (101)	angled eq. (103)	pitch. eq. (104)	struc. eq. (105)	theory total, 5-part	experiment
8	8.57	2.61	.44	.40	1.20	13.22	16.1
10	8.04	2.23	.42	.31	.93	11.93	13.3
12	7.70	1.92	.42	.25	.75	11.04	11.6
14	7.52	1.67	.45	.20	.60	10.44	9.8
16	7.44	1.46	.50	.16	.48	10.04	10.7
18	7.45	1.27	.58	.13	.39	9.82	9.7
20	7.55	1.12	.68	.11	.33	9.79	10.5
22	7.71	.97	.86	.09	.27	9.90	8.7

The proportion of power expenditure due to vibratory-swirl is relatively large and it appears this could be reduced by synchronized counterrotating blades, that is, blades positioned so that maximum swirl is nullified.

COUNTERROTATING PROPELLERS AND OTHER CONFIGURATIONS FOR ISOLATING CYCLIC-CONTROL FORCES AND MOMENTS

In any control system it is desirable to initiate a given force or moment without other accompanying forces and moments. For example, to initiate pitching moment without side force or thrust change, that is, to isolate pitching moment from the other control forces and moments.

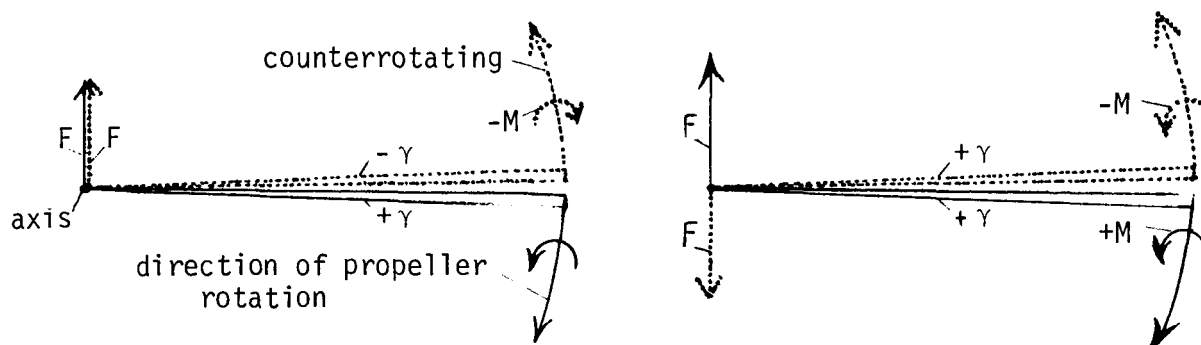
A single propeller with cyclic-control generates a moment and a force and neither can be isolated. As shown here schematically, a positive γ applied to gain pitching, also gains a side force. The side force comes from the reaction to the increased torque on the blade when the blade is at a $\beta_0 + \gamma$ angle at $\psi = \pi$. The + sign indicates a positive moment where γ maximizes the blade angle. This single propeller effect, of forces and moments which cannot be isolated, can be seen analytically in equations (75) and (76). For any value of azimuth angle in these equations, there will be a force and moment



combination. However, the counterrotating propeller has unique cyclic-control qualities of isolating control forces and moments, and in addition, rolling moment control, that is, moments about the axis. Multi-propellers, in-line, can also isolate forces and moments.

Counterrotating Propeller

Two blades of the counterrotating propeller with cyclic-control, at two different operating modes, are shown in aft view as follows:



In the left drawing, with a plus cyclic-angle γ on one blade and a negative angle γ on the counterrotating blade, the moments cancel, while the reaction forces add and provide a net translation force. In the right drawing, a plus angle γ on both the downgoing blade and the counterrotating blade results in a cancellation of forces and the moments add to provide a net moment on the propeller plane. Since azimuth angle ψ is not specified in this example, then the results apply at any azimuth angle, hence with an azimuth control angle, forces and moments can be controlled singularly or jointly in any direction in the propeller plane. Thus the cyclic-control counterrotating propeller has a built-in capability of isolating all forces and moments or combinations, without the need of propeller tilt or of net thrust changes. The above left drawing can be considered as a rotor in a horizontal plane, that is, helicopter mode, then the cyclic-control force becomes a direction-controllable propulsive force while the rotor remains horizontal, or untilted. For this configuration the rolling moment, that is, a moment about the propeller axis or shaft, is equal to a torque differential made by a blade angle difference between the two rotors.

Cyclic-control analysis. - The analysis developed for the single propeller can be applied to the counterrotating propeller by taking into account the azimuth angle for control. From equation (1) it can be seen that the azimuth control angle is linearly proportional to ψ_0 , hence, ψ_0 will be used as a displaced control angle. The cyclic-control solutions with sinusoidal cycle, $f(\psi - \psi_0) = \cos(\psi - \psi_0)$, for the single propeller are given in equations (73) through (76). For the counterrotating propeller let subscript 1 refer to the rotor with clockwise rotation, and subscript 2 to the rotor with counterclockwise rotation. Then equation (73) applied to each of the two rotors becomes

$$C_{Tav1} - C_{T1} = \frac{1}{4} \gamma_1^2 C_{T1}^{*''}, \quad C_{Tav2} - C_{T2} = \frac{1}{4} \gamma_2^2 C_{T2}^{*''}$$

Adding these two equations gives

$$C_{Tav} - C_T = \frac{1}{4} (\gamma_1^2 C_{T1}^{*''} + \gamma_2^2 C_{T2}^{*''}) \quad (107)$$

For equal and equal operating clockwise and counterclockwise rotating rotors

$$C_{T1}^{*''} = C_{T2}^{*''} = C_T^{*''}/2$$

Then

$$\frac{C_{Tav} - C_T}{C_T} = \frac{1}{8} (\gamma_1^2 + \gamma_2^2) \frac{C_T^{*''}}{C_T} \quad (108)$$

where these thrust coefficients and derivatives are of the counterrotating propeller. Similarly, for the power change

$$(C_{P_{av}} - C_P)_{ideal} = \frac{1}{4} (\gamma_1^2 C_{P1}^{*''} + \gamma_2^2 C_{P2}^{*''}) \quad (109)$$

$$\left(\frac{C_{P_{av}} - C_P}{C_P} \right)_{ideal} = \frac{1}{8} (\gamma_1^2 + \gamma_2^2) \frac{C_P^{*''}}{C_P} \quad (110)$$

When $\gamma_1 = \gamma_2 = \gamma$, equations (108) and (110) become the same equations as those for the single propeller.

From equations (75) and (76), define K's as

$$K_m = \frac{1}{4} \left(\rho_T^* \frac{C_T^{*'}}{C_T} + \frac{C_T^*}{C_T} \rho_T^{*'} \right) \quad (111)$$

$$K_\gamma = \frac{1}{2\pi} \left[\frac{1}{\rho_P} \frac{C_P'}{C_P} + \left(\frac{1}{\rho_P} \right)' \right] \quad (112)$$

From equation (75), for each of the rotors

$$C_{m1} = -C_{T1} K_{m1} \gamma_1 \cos \psi_{01}, \quad C_{m2} = -C_{T2} K_{m2} \gamma_2 \cos \psi_{02}$$

Then adding

$$C_m = -[C_{T1}K_{m1}\gamma_1\cos\psi_{01} + C_{T2}K_{m2}\gamma_2\cos\psi_{02}] \quad (113)$$

Similarly, then

$$C_n = -[C_{T1}K_{m1}\gamma_1\sin\psi_{01} + C_{T2}K_{m2}\gamma_2\sin\psi_{02}] \quad (114)$$

With the same procedure, using equation (76)

$$C_Y = -[C_{P1}K_{Y1}\gamma_1\cos\psi_{01} - C_{P2}K_{Y2}\gamma_2\cos\psi_{02}] \quad (115)$$

$$C_N = C_{P1}K_{Y1}\gamma_1\sin\psi_{01} - C_{P2}K_{Y2}\gamma_2\sin\psi_{02} \quad (116)$$

where the negative signs of the second terms are because the torque reaction force of counterclockwise rotation is in opposite direction to that with clockwise rotation. For equal and equal operating clockwise and counterclockwise rotation rotors

$$\left. \begin{aligned} C_{T1} &= C_{T2} = C_T/2, & C_{P1} &= C_{P2} = C_P/2 \\ K_{m1} &= K_{m2} = K_m, & K_{Y1} &= K_{Y2} = K_Y \end{aligned} \right\} \quad (117)$$

then equations (113) through (116) become

$$\frac{C_m}{C_T} = -\frac{1}{2} K_m (\gamma_1 \cos\psi_{01} + \gamma_2 \cos\psi_{02}) \quad (118)$$

$$\frac{C_n}{C_T} = -\frac{1}{2} K_m (\gamma_1 \sin\psi_{01} + \gamma_2 \sin\psi_{02}) \quad (119)$$

$$\frac{C_Y}{C_P} = -\frac{1}{2} K_Y (\gamma_1 \cos\psi_{01} - \gamma_2 \cos\psi_{02}) \quad (120)$$

$$\frac{C_N}{C_P} = \frac{1}{2} K_Y (\gamma_1 \sin\psi_{01} - \gamma_2 \sin\psi_{02}) \quad (121)$$

For isolating the forces from the moments, the terms within the parenthesis of equations (118) and (119), must be zero. Then

$$\frac{\gamma_2}{\gamma_1} = \frac{-\cos\psi_{01}}{\cos\psi_{02}} = \frac{\cos(\pi + \psi_{01})}{\cos\psi_{02}}, \quad \frac{\gamma_2}{\gamma_1} = \frac{-\sin\psi_{01}}{\sin\psi_{02}} = \frac{\sin(\pi + \psi_{01})}{\sin\psi_{02}}$$

Equating these two equations, Ψ_{02} can be evaluated as

$$\Psi_{02} = \pi + \Psi_{01}, \text{ then } \gamma_2 \equiv \gamma_1 \quad (122)$$

Similarly, for isolating the moments from the forces, the values within the parentheses of equations (120) and (121) must be zero. The solution gives

$$\Psi_{02} = \Psi_{01}, \text{ then } \gamma_2 = \gamma_1 \quad (123)$$

Thus, when the cyclic-blade angle magnitude is the same on both rotors, the cyclic-control forces and moments can be isolated with a counterrotating propeller by the azimuth control angle on each rotor. With $\gamma_1 = \gamma_2 = \gamma$, equations (118) through (121) become

$$\frac{C_{m\gamma}}{C_T} = -\frac{1}{2} K_m (\cos \Psi_{01} + \cos \Psi_{02}) \quad (124)$$

$$\frac{C_{n\gamma}}{C_T} = -\frac{1}{2} K_m (\sin \Psi_{01} + \sin \Psi_{02}) \quad (125)$$

$$\frac{C_Y}{C_P} = -\frac{1}{2} K_Y (\cos \Psi_{01} - \cos \Psi_{02}) \quad (126)$$

$$\frac{C_N}{C_P} = \frac{1}{2} K_Y (\sin \Psi_{01} - \sin \Psi_{02}) \quad (127)$$

where Ψ_{01} is the Ψ_0 of the rotor with clockwise rotation, and Ψ_{02} is the Ψ_0 of the rotor with counterclockwise rotation. The K's are given in equations (111) and (112).

The rolling moment coefficient about the propeller axis or shaft is

$$C_r = \frac{L}{\rho_a n^2 D^5} = -\frac{1}{4\pi} [C_P(\beta_0 + \gamma_1) - C_P(\beta_0 - \gamma_2)] \quad (128)$$

where the blade angle of rotor 1 is increased by the angle γ_1 , and of rotor 2 decreased by γ_2 , where L is the rolling moment, and the parentheses represent functional parameters of the power coefficient. Equation (128) is the change in torque between one rotor and the other, then

$$C_r = -\Delta C_Q = -\frac{\Delta C_P}{2\pi} = -\frac{1}{2\pi}[C_{P_1}(\beta_0 + \gamma_1) - C_{P_2}(\beta_0 - \gamma_2)]$$

which with $C_{P_1} = C_{P_2} = C_P/2$ for equal rotors, leads to equation (128).

Equations (124) through (127) are such that any arbitrary control force, moment, or combination can be initiated by the azimuth angle control of ψ_{01} and ψ_{02} . For the case of isolated moments, $\psi_{02} = \psi_{01}$, then

$$C_Y = C_N = 0, \quad \frac{C_{m_Y}}{C_T} = -K_m \cos \psi_{01}, \quad \frac{C_{n_Y}}{C_T} = -K_m \sin \psi_{01} \quad (129)$$

The resultant moment is

$$\frac{C_{mn_Y}}{C_T} = \frac{(C_{m_Y}^2 + C_{n_Y}^2)^{1/2}}{C_T} = K_m, \quad \text{at } \psi_{mn} = \psi_{01} \quad (130)$$

where ψ_{mn} is from $\tan \psi_{mn} = C_{n_Y}/C_{m_Y}$. This resultant moment is acting forward and normal to the propeller disc at azimuth angle ψ_{01} . For the case of isolated forces, $\psi_{02} = \pi + \psi_{01}$, then from equations (124) through (127)

$$C_m = C_n = 0, \quad \frac{C_{Y_Y}}{C_P} = -K_Y \cos \psi_{01}, \quad \frac{C_{N_Y}}{C_P} = K_Y \sin \psi_{01} \quad (131)$$

The resultant force is

$$\frac{C_{YN_Y}}{C_P} = \frac{(C_{Y_Y}^2 + C_{N_Y}^2)^{1/2}}{C_P} = K_Y, \quad \text{at } \psi_{YN} = -\psi_{01} \quad (132)$$

where ψ_{YN} is from $\tan \psi_{YN} = C_{N_Y}/C_{Y_Y}$. This resultant force is acting radially outward from the shaft at azimuth angle ψ_{YN} . Thus to isolate moments, ψ_{02} is set equal to ψ_{01} , and to isolate forces, ψ_{02} is set equal to $\pi + \psi_{01}$, and ψ_{01} is controllable through the ψ_{con} control angle in equation (1).

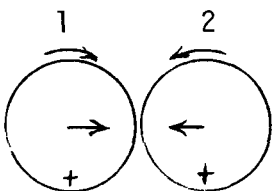
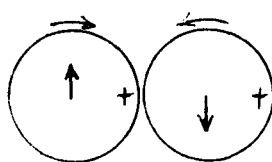
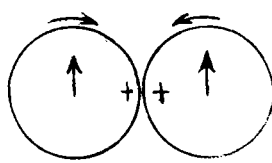
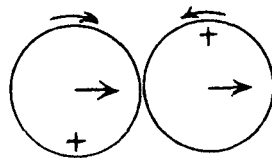
The cyclic-control analysis for the counterrotating propeller include equations (108) and (110) of the change in thrust and power, equations (124) through (127) of cyclic-control forces and moments, equation (128) of rolling moment by blade angle differential, and equations (130) and (132) of isolated cyclic-control moment and force. The K_m and K_Y functions are given in equations (111) and (112). The extra power required in cyclic-control operation, approximated in equations (100), (103), (104), and (105), apply also to the counterrotating propeller, except for the isolated moment condition. For this condition the vibratory swirl from the two rotors cancel each other and equation (100) is assumed zero. In the isolated moment condition, $C_Y = C_N = 0$, then equation (103), angled slipstream power, becomes zero. Since force along the propeller

axis, that is, thrust, is simply controlled by steady-state blade angle, then six degrees of freedom are controllable with a cyclic-control counterrotating propeller.

Unique cyclic-control characteristics. - The counterrotating propeller capability for isolating six control forces and moments is particularly ideal for large lifting-crane type vehicles, for airship and submarine control, and for tilt rotors. The lifting-crane helicopter can be made to generate a propulsive force in any horizontal direction by isolating the side and normal forces, done without tilting the rotor. For hovering, the six degree of freedom direct control can be maintained without any movement of the aircraft, making it an exceptionally stable platform. For the same reasons, a cyclic-control counterrotating propeller, concentric at the tail of an airship or submarine, can control the hover of these vehicles without vehicle movement, or at forward velocities can provide six degree of freedom direct control.

Multipropellers In Line


Single rotation propellers when in line as on a planar wing, can be operated so that some or all the control forces and moments can be isolated. Examination of control forces and moments can be made from drawings of the propeller disc, represented by a circle depicting an aft view of the disc. The curved arrow on top of the disc indicates the direction of propeller rotation, the straight arrow indicates control force, the + sign shows position of cyclic-angle γ , and the control moment acts out of the page at azimuth angle position denoted by +. Results for two propellers in line are as follows:

to isolate pitching:	with equal γ , side forces are cancelled.	
yawing and rolling:	cannot be isolated.	
normal force:	with equal γ , yawing and rolling are cancelled	
side force:	with equal γ , pitching is cancelled	

Hence, for two propellers, all control forces and moments can be isolated except yawing from rolling.

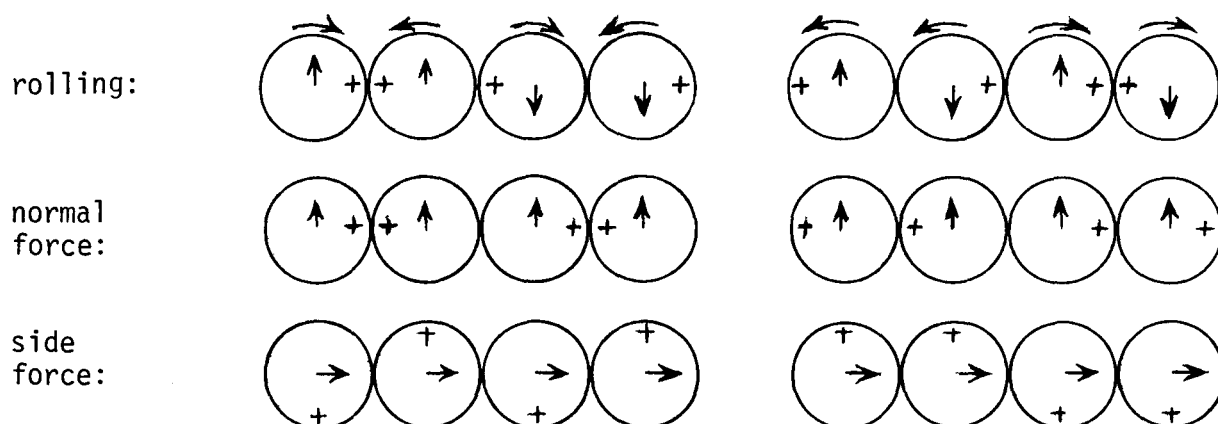
Results for three propellers in line, are

		1	2	3
to isolate pitching:	with $\gamma_2 = \gamma_1 + \gamma_3$, $\gamma_1 = \gamma_3$, side force and yawing cancel			
yawing:	with $\gamma_2 = \gamma_1 + \gamma_3$, $\gamma_1 = \gamma_3$, normal force and rolling cancel			
rolling:	with $\gamma_2 = 0$, $\gamma_1 = \gamma_3$, normal force and yawing cancel			
normal force:	with $\gamma_2 = \gamma_1 + \gamma_3$, $\gamma_1 = \gamma_3$, yawing and rolling cancel			
side force:	with $\gamma_2 = \gamma_1 + \gamma_3$, pitching is cancelled			

With three propellers, propeller rotation given by the sense  can also isolate control forces and moments, however, the relationship between, $\gamma_1, \gamma_2, \gamma_3$ for isolating rolling, becomes complicated; also, the yawing ability is weak since it would be only that due to the center propeller moment arm offset.

Results for four propellers in line, are

to isolate pitching:		
yawing:		



With four in line propellers, the rotation sequence, $\curvearrowright \curvearrowleft \curvearrowright \curvearrowleft$, of the group on the left is preferred because the isolated yawing moment magnitude is twice that obtained from the rotation of the group on the right. The other isolated control forces and moments are the same in either group.

In all of the above configurations, an opposite propeller rotation leads to the same result, except the directions of the straight arrows are opposite, leading to some sign changes in the forces and moments. It can be noted that three is the minimum number of propellers grouped laterally which can, by cyclic-control, isolate all the control forces and moments. Cyclic-control analysis for each of the propellers in a multipropeller group is assumed to be the same as for the single propeller analysis given in equations (73) through (76). Greater accuracy is possible if the steady-state C_T and C_P versus blade angle values are known for each propeller in a multipropeller group.

RESULTS AND DISCUSSION

Guide for Usage of Theory

The theoretical cyclic-control equations are derived as a generalized theory relating cyclic-control forces, moments, power, and thrust changes, to the steady-state characteristics of the same propeller. For each cyclic-controlled propeller there are two arbitrary controls. These include the cyclic-blade angle γ , for governing the magnitude of the cyclic-control force or moment, and the azimuth control angle, ψ_{con} , for governing the direction or sense of the cyclic-control force or moment.

Sinusoidal cycle. - For the cyclic-blade angle which varies sinusoidally with azimuth angle, the cyclic function is $f(\psi - \psi_0) = \cos(\psi - \psi_0)$, then with angle γ not large, the cyclic-control relations are given in equations (73) through (76). These relations are most useful, and are theoretically accurate but analytically simple. Equations (40) through (43) apply for the condition of large γ . For the sinusoidal cycle the IP_n and IM_n are evaluated by substituting n for a in equations (28) and (29), then $IP_n = 1, 3/4, 5/8, 35/64, \dots, (n-1)IP_{n-2}/n, n = 2, 4, 6, \dots, \text{even}$, and $IM_n/\cos\psi_0 = 1, 3/4, 5/8, 35/64, \dots, nIM_{n-2}/(n+1)\cos\psi_0, n = 1, 3, 5, \dots, \text{odd}$.

The cyclic-control solution in terms of Bessel functions represents a closed function solution for any value of γ . This solution is in terms of the Fourier coefficients of the steady-state thrust and power and radial centers of thrust and power. The linear-with-J steady-state thrust coefficient is represented in a Fourier series in β_0 as in equation (45). Then the cyclic-control change in thrust is given in equation (50), and the moments C_m and C_n are given in equations (55) and (5). Similarly, with the steady-state power coefficient represented in equation (51) as a Fourier series, the cyclic-control ideal change in power is given in equation (52), and the forces C_Y and C_N are given in equations (59) and (7). The blade angle variation in a cycle is given in equation (46) where ψ_0 from equation (1) includes the azimuth control angle ψ_{con} .

An alternative solution in terms of Bessel functions is as follows. If the steady-state theoretical or experimental data includes the blade radial center of thrust, then the product $\rho_T^* C_T^*$ can be expressed as a Fourier series, given as

$$\rho_T^* C_T^* = \sum_{n=0}^{\infty} (e_n \cos n\beta_0 + f_n \sin n\beta_0) \quad (133)$$

where e_n and f_n are Fourier coefficients. The cyclic-control solution for C_m is the same as that of equation (55) except e_n and f_n replace a_n and b_n , and since ρ_T^* is part of equation (133), $K_T = 0$, $\rho_T^* = 1$, then equation (55) becomes

$$C_m = C_n \cot \psi_0 = \frac{1}{2} \cos \psi_0 \sum_{n=1}^{\infty} (-e_n \sin n\beta_0 + f_n \cos n\beta_0) J_1(n\gamma) \quad (134)$$

Similarly, for C_p/ρ_p expanded in a Fourier series

$$\frac{C_p}{\rho_p} = \sum_{n=0}^{\infty} (g_n \cos n\beta_0 + h_n \sin n\beta_0) \quad (135)$$

then with equation (59)

$$C_Y = -C_N \cot \psi_0 = \frac{1}{\pi} \cos \psi_0 \sum_{n=1}^{\infty} (-g_n \sin n\beta_0 + h_n \cos n\beta_0) J_1(n\gamma) \quad (136)$$

Steady-state propeller data. - Propeller theoretical or experimental performance charts contain C_T and C_p as functions of advance ratio. From the $C_T \sim J$ chart, C_T^* from equation (B18) can be evaluated as a function of steady-state blade angle, β_0 . With the $C_T^*(\beta_0)$ function known, the derivatives of C_T^* with respect to β_0 , or C_T^* as a Fourier series in β_0 , can be formulated for use in the cyclic-control theory. Similarly, for a given value of J , the $C_p(\beta_0)$ function is known, then the derivatives of C_p with respect to β_0 , or C_p as a Fourier series in β_0 , can be formulated. An approximation for the radial center of thrust is given in equation (53) and its derivative in equation (81). A similar approximate expression for radial center of power or

torque is given in equation (57) and its derivative in equation (93). Propeller performance data, particularly theoretical, can include the change of thrust and power with change in radius, as a function of blade radius position. Then the radial centers of thrust and power as functions of β_0 are given directly for application in the cyclic-control solution equations.

An alternative but approximate steady-state solution is presented in appendix B. The first and second partial derivatives of the thrust coefficient are given in equations (B16) and (B17). Equation (B17) into (73) gives the cyclic-control thrust change, and equations (B16), (B10), (53), with (75) gives the cyclic-control moments. The first and second partial derivatives of the power coefficient are given in equations (B23) and (B24), which when $J = 0$, simplify to those in equations (B31) and (B32). With equation (57), the ideal power change and cyclic-control forces are determined from equations (74) and (76).

Arbitrary cyclic function. - The cyclic function is $f(\psi - \psi_0)$ defined in equation (11). The cyclic function can be any arbitrary antisymmetric function with azimuth angle, but by definition, bounded within ± 1 . The generalized cyclic-control solution for an arbitrary cyclic function is given in equations (40) through (43). Example solutions of arbitrary cyclic functions are given in the section, Cyclic function of cosine to m-power.

Extra power changes. - The total power change due to cyclic-control is the sum of ideal power change plus extra power changes which include vibratory swirl of the slipstream, angled slipstream, pitching airfoil of the propeller blades, and vibratory structural damping. An estimate of these extra power expenditures can be made from equations (100), (103), (104), and (105), respectively.

Counterrotating propeller. - With the condition that each rotor has the same value of γ , the cyclic-control pitching and yawing moments are given in equations (124) and (125) and side and normal forces in equations (126) and (127). When moments are isolated, that is, forces are zero, the resultant moment is given in equation (130) at a given azimuth angle. When forces are isolated, that is, moments are zero, the resultant force is given in equation (132) directed radial outward from the shaft at a given azimuth angle. The thrust change is given in equation (108), and the ideal power change in equation (110). The rolling moment about the propeller shaft is the change of torque between the two rotors, given in equation (128). The longitudinal force along the propeller axis, or thrust, is simply controlled by steady-state blade angle. The extra power required in cyclic-control operation is approximated in equations (100), (103), (104), and (105). However, in the isolated moment condition the vibratory swirl from the two rotors cancel each other and equation (100) is assumed zero. Also in the isolated moment condition, the forces are zero, then equation (103) becomes zero.

Example Solution and Experimental Comparison

An example use of cyclic-control theory is shown by applying the theory to a test-model propeller. The theory is given in equations (73) through (76). The geometric characteristics of the propeller are listed in equation (77). Analytical analysis of the test steady-state thrust and power data results in functional relationships with blade angle. Taking derivatives with respect to blade angle provides the thrust and power derivatives. These derivatives could have been obtained graphically from curves of steady-state thrust and power against blade angle. These thrust derivatives are $J = 0$ values, but not the linear-with- J values. The tests were made at $J = 0$, thus the thrust starred value of equation (B18) remains unknown. For this case an estimate of the thrust starred derivatives is given in equations (B19) and (B20), in terms of thrust derivatives at $J = 0$. With the derivatives known and with equations (53) and (57), the cyclic-control values are determined from equations (73) through (76). Details of the theory application are given in the section titled, Comparison of Theory with Experiment. In that section, theory values of thrust change and pitching moment are compared with experiment, for various values of blade angle. The theory and test results correlate within the accuracy of the test measurements. Similar correlation is shown for the side force prediction. The theoretical ideal change of power is of the order 30 percent less than the total measured change of power. Extra power values are estimated in the section titled, Total Power Comparisons of Theory with Experiment, which shows good correlation between theory and experiment of total power change due to cyclic-control. In comparison with the four extra power estimates, the slipstream vibratory swirl power due to cyclic control appears as the largest.

Isolated Cyclic-Control Forces and Moments

In an aircraft control system it is desirable to initiate a given force or moment without other accompanying forces or moments. The cyclic-control counter-rotating propeller has this unique quality as shown in the development given in the section, Counterrotating Propeller. Qualitatively, isolation of forces and moments are demonstrated at the beginning of that section, and analytically in equations (124) through (127). The control is by means of the azimuth angle of each rotor. When ψ_{02} of rotor 2 is set equal to ψ_{01} of rotor 1, then the forces are zero and the moments are isolated. When ψ_{02} is set equal to $\pi + \psi_{01}$, then the moments are zero and the forces are isolated.

Concurrent control of arbitrary force and moment of a counterrotating propeller. - Equations (118) through (121) apply for equal steady-state operation of the clockwise rotation rotor 1, and the counterclockwise rotation rotor 2. The resultants of arbitrary moment and of force are given by

$$\left. \begin{aligned} C_{mn} &= (C_m^2 + C_n^2)^{1/2}, \text{ at } \psi_{mn} = k_n \pi + \tan^{-1} \frac{C_n}{C_m} \\ \text{where } k_n &= \frac{C_n}{2|C_n|} \left(1 - \frac{C_m}{|C_m|} \right) \end{aligned} \right\} \quad (137)$$

$$\left. \begin{aligned} C_{YN} &= (C_Y^2 + C_N^2)^{1/2}, \text{ at } \psi_{YN} = k_Y \pi + \tan^{-1} \frac{C_Y}{C_N} \\ \text{where } k_Y &= \frac{C_Y}{2|C_Y|} \left(1 - \frac{C_N}{|C_N|}\right) \end{aligned} \right\} \quad (138)$$

The desired moment, force, and directions are C_{mn} , ψ_{mn} , C_{YN} , and ψ_{YN} . The clockwise rotation rotor and the counterclockwise rotation rotor respectfully have the cyclic-blade angle variation given by

$$\beta_1 = \beta_0 + \gamma_1 \cos (\psi - \psi_{01}) \quad (139)$$

$$\beta_2 = \beta_0 + \gamma_2 \cos (\psi - \psi_{02}) \quad (140)$$

For given values of γ_1 , ψ_{01} , γ_2 , and ψ_{02} , the C_m , C_n , C_Y , and C_N coefficients are determined from equations (118) through (121). With these values, the resultant moment and force are obtained from equations (137) and (138). In the application for isolating force and moment resultants from each other, the γ -angles become $\gamma_2 = \gamma_1$, then equations (137) and (138) simplify to the solutions of equations (130) and (132).

Multipropeller. - The forces and moments of a single propeller with cyclic-control cannot be isolated. In the section, Multipropellers In Line, it is shown how for two propellers in line as on a wing, the pitching moment and side and normal forces can be isolated, but yawing and rolling moments cannot. Three propellers in line is the minimum number for which all forces and moments can be isolated. For propellers in line the direction of propeller rotation of one propeller relative to the next, influences the magnitude of the isolated yawing and rolling moments.

Effect of Cyclic Function

Cyclic functions, $f(\psi - \psi_0)$, other than sinusoidal are investigated in the sections Cyclic function of cosine to m-power and Cyclic function for most moment with least extra power, also, with minimum blade pitching acceleration. The results show that when the cyclic function is a step function then the cyclic-control forces and moments are maximum, 27 percent larger than for the sinusoidal cyclic function. The ideal change in power is twice larger than that for the sinusoidal cycle. The step function means that blade angle is $\beta_0 + \gamma$ for half a cycle and $\beta_0 - \gamma$ for the second half, which results in an infinite blade angle acceleration at each change. The largest cyclic-control force or moment for a given ideal change of power is shown to be a cyclic function which is sinusoidal. Blade fatigue depends on the maximum blade angular acceleration. The cyclic function which has the smallest maximum acceleration has ten percent less than that of the sinusoidal cycle and is given in equation (39). This function is very close to sinusoidal and the force or moment to power ratio is essentially the same as that of the sinusoidal cycle.

Propeller Inclination

Propeller forces and moments and thrust and power changes are generated when the propeller is inclined to the free-stream velocity. These values are obtainable from the theory of reference 4. It is the derivatives with respect to blade angle of the steady-state thrust and power of the inclined propeller which are used for application in the present cyclic-control theory. The total propeller forces and moments are those due to cyclic-control plus those due to inclination angle.

CONCLUSIONS

The equations for forces and moments, and thrust and power changes, due to a cyclic-controlled propeller, when analytically derived by power series, have led to a mathematical classic in simplicity. These cyclic-control equations are directly related to the derivative with respect to blade angle of the steady-state propeller thrust and power characteristics. The solution remains simple for any harmonic variation of cyclic-blade angle with azimuth angle during the blade revolution. An alternative solution, limited to sinusoidal variation of cyclic-blade angle, is in terms of Bessel functions, which results in a closed-form solution for any value of maximum cyclic-blade angle. The study shows that a sinusoidal variation of cyclic-blade angle gives the maximum control force and moment for a given ideal change in power. A step variation of cyclic-blade angle gives the maximum control force and moment, which is 27 percent greater than that of sinusoidal variation, however, the ideal change in power is twice larger. A sinusoidal cycle with a small third harmonic is as effective as the sinusoidal alone, but has ten percent less maximum angular acceleration which may be a fatigue consideration. Analyses for estimating four extra power required terms show that the slipstream vibratory swirl excited by cyclic actions adds 15 to 20 percent to the ideal change in power, while several other contributors to power remain small. An example application of the theory to a cyclic-control test propeller shows good correlation between theory and test results of cyclic-control force and moment, and power and thrust change.

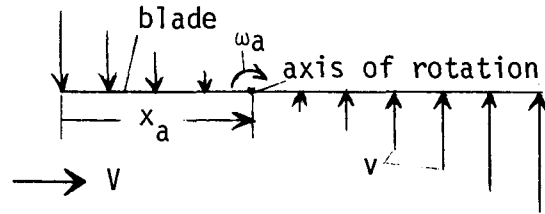
Cyclic-control analysis is developed for the counterrotating propeller. It is shown that uniquely, a single counterrotating propeller can isolate all cyclic-control forces and moments, thus this propeller makes an ideal powered control, active control, and propulsive unit for a vehicle. A minimum of three and preferably four propellers in line, as on a wing, are needed to isolate all cyclic-control forces and moments.

KENTRON INTERNATIONAL, INC.
Hampton Technical Center
an LTV company
Hampton, Virginia 23666
May 2, 1979

APPENDIX A

QUASI-STEADY AZIMUTH ANGLE CHANGE DUE TO BLADE CYCLIC PITCHING AT CHORD POSITION ξ_a

For a blade that pitches about an axis x_a distance from the leading edge, a linear with x velocity is induced along the blade chord, as shown in the drawing. This induced velocity creates an induced camber on the blade which is positive for plus ω_a , and is a negative camber when ω_a is negative. This camber changes the blade loading and lift, thus



$$\frac{d\ell}{dx} = \frac{1}{2} \rho_a V^2 b c_{\ell_\alpha} (\alpha_0 + \frac{v}{V}) \quad (A1)$$

The quasi-steady solution assumes that the lift is that with ω_a as a constant. The induced velocity is

$$\frac{v}{V} = \frac{b\omega_a}{V} (\xi - \xi_a) \quad (A2)$$

where b is blade chord, $\xi = x/b$, $\xi_a = x_a/b$. The thin-airfoil solution for lift of the blade with this induced velocity is

$$c_{\ell} = 2\pi \left[\alpha_0 + \frac{b\omega_a}{V} \left(\frac{3}{4} - \xi_a \right) \right] \quad (A3)$$

The value within the brackets represents the effective blade angle which for cyclic control becomes

$$\beta_0 + \gamma f(\Psi - \Psi_0) = \beta_0 + \gamma f(\Psi - \Psi_1) + \frac{b\omega_a}{V_R} \left(\frac{3}{4} - \xi_a \right) \quad (A4)$$

where

$$V_R = \frac{2\pi n r}{\cos \phi}, \quad \Psi_1 = \Psi_{ph} + \Psi_{con} \quad (A5)$$

The angular velocity of a cyclic-control blade is the derivative of equation (A4) with respect to time, then

$$\omega_a = \frac{d\beta_0}{dt} + \frac{d\gamma}{dt} f(\Psi - \Psi_1) + \gamma \frac{df(\Psi - \Psi_1)}{dt} + \frac{b}{V_R} \left(\frac{3}{4} - \xi_a \right) \frac{d\omega_a}{dt}$$

which since β_0 , γ , and ω_a are assumed constant with time, becomes

$$\omega_a = \gamma \frac{df(\Psi - \Psi_1)}{d(\Psi - \Psi_1)} \frac{d(\Psi - \Psi_1)}{dt} = 2\pi n \gamma \frac{df(\Psi - \Psi_1)}{d(\Psi - \Psi_1)} \quad (A6)$$

Also, at $r = \frac{3}{4} R$

$$V_R \cong \frac{3}{2} \pi n R [1 + (\frac{4J}{3\pi})^2]^{1/2}, \quad b = \frac{3}{2} \pi R \frac{\sigma}{B} \quad (A7)$$

Combining equations (A6) and (A7) results in

$$\frac{b\omega_a}{V_R} = \frac{2\pi \frac{\sigma}{B} \gamma}{[1 + (\frac{4J}{3\pi})^2]^{1/2}} \frac{df(\Psi - \Psi_1)}{d(\Psi - \Psi_1)} \quad (A8)$$

Equation (A8) is inserted into the effective blade angle equation (A4), then

$$f(\Psi - \Psi_0) = f(\Psi - \Psi_1) + \frac{2\pi \frac{\sigma}{B} (\frac{3}{4} - \xi_a)}{[1 + (\frac{4J}{3\pi})^2]^{1/2}} \frac{df(\Psi - \Psi_1)}{d(\Psi - \Psi_1)} \quad (A9)$$

which shows angular change due to the derivative term. For sinusoidal blade variation, $f(\Psi - \Psi_1) = \cos(\Psi - \Psi_1)$, then

$$\cos(\Psi - \Psi_0) = \cos(\Psi - \Psi_1) - \frac{2\pi \frac{\sigma}{B} (\frac{3}{4} - \xi_a)}{[1 + (\frac{4J}{3\pi})^2]^{1/2}} \sin(\Psi - \Psi_1) \quad (A10)$$

$$= \left\{ 1 + \frac{[2\pi \frac{\sigma}{B} (\frac{3}{4} - \xi_a)]^2}{1 + (\frac{4J}{3\pi})^2} \right\}^{1/2} \cos \left\{ \Psi - \Psi_1 + \tan^{-1} \frac{2\pi \frac{\sigma}{B} (\frac{3}{4} - \xi_a)}{[1 + (\frac{4J}{3\pi})^2]^{1/2}} \right\}$$

Since $(\sigma/B)^2$ is small, the factor of the cosine term is approximately unity, then with equations (1) and (A5), equation (A10) simplifies to

$$\Psi_{ax}(\xi_a) = -\tan^{-1} \frac{2\pi \frac{\sigma}{B} (\frac{3}{4} - \xi_a)}{[1 + (\frac{4J}{3\pi})^2]^{1/2}} \quad (A11)$$

The effective ψ_{ax} is $\psi_{ax}(\xi_a) - \psi_{ax}(\frac{1}{4})$, then

$$\psi_{ax} = \tan^{-1} \frac{2\pi \frac{\sigma}{B} (\xi_a - \frac{1}{4})}{[1 + (\frac{4J}{3\pi})^2]^{1/2}} \quad (A12)$$

where $\xi_a = x_a/b$ is the blade chord position from blade leading edge about which the blade pitches, typically $\xi_a \approx 1/2$. The effective phase angle change, ψ_{ax} , due to blade pitching at arbitrary values of ξ_a , will not be large since the ratio of propeller solidity to number of blades is small.

APPENDIX B

APPROXIMATE STEADY-STATE PROPELLER THRUST AND POWER COEFFICIENTS AND DERIVATIVES

From reference 4 the linear with advance ratio approximations of thrust and power coefficients are

$$C_T^* = e_T(J_{0T} - J)\cos(\beta_0 - \epsilon) \quad (B1)$$

$$C_P^* = e_P(J_{0P} - J)\sin\beta_0 \quad (B2)$$

where

$$e_T = \frac{4.6 \kappa \sigma}{1 + (3 + \frac{9}{B}) \kappa \sigma} \quad (B3)$$

$$e_P = \frac{10.4 \kappa \sigma}{1 + (1 + \frac{24}{B}) \kappa \sigma} \quad (B4)$$

$$J_{0T} = g \tan \beta_0 \quad (B5)$$

$$g = 2.1 + .5 \tan \beta_1 \quad (B6)$$

$$J_{0P} = J_{0T} + h \quad (B7)$$

$$h = \frac{8 d_0 [1 + 7 \sin^2 3(\beta_0 - \beta_1)]}{15 \sin \beta_0 \cos^3 \beta_0} \quad (B8)$$

$$d_0 = \delta_0 + .8(\delta_0 + \frac{3\kappa\sigma}{B})\sin^2 \beta_1 \quad (B9)$$

where κ is blade section lift coefficient divided by 2π , B is number of blades, δ_0 is blade section drag coefficient at zero lift, and β_1 is given in equation (54). The nonlinear variation with advance ratio is approximated by a square root factor, as

$$C_T = \frac{C_T^*}{E_T^{1/2}} \quad (B10)$$

$$C_P = \frac{C_P^*}{E_P^{1/2}} \quad (B11)$$

where

$$E_T = 1 + \frac{25}{4} e_T^2 (1 + \frac{3}{8} \sin 2\beta_0)^2 (1 - \frac{J}{J_{0T}})^2 \quad (B12)$$

$$E_P = 1 + 9 e_P^2 (1 - \frac{J}{J_{0P}})^2 \quad (B13)$$

Thrust Coefficient Derivatives

The ratios of C_T^*/C_T , and $C_T^{*''}/C_T$ are needed. The single prime and double prime indicate the first partial derivative and the second partial derivative with respect to β_0 . From equation (B5)

$$J_{0T}' = \frac{2J_{0T}}{\sin 2\beta_0} = \frac{g}{\cos^2 \beta_0} \quad (B14)$$

$$J_{0T}'' = \frac{2J_{0T}}{\cos^2 \beta_0} = \frac{2g \sin \beta_0}{\cos^3 \beta_0} \quad (B15)$$

then the first derivative of equation (B1), divided by C_T , is

$$\frac{C_T^*'}{C_T} = \left[\frac{2J_{0T}}{(J_{0T} - J) \sin 2\beta_0} - \tan(\beta_0 - \epsilon) \right] E_T^{1/2} \quad (B16)$$

The second derivative of equation (B1), divided by C_T , is

$$\frac{C_T^{*''}}{C_T} = \left[-1 + \frac{2J_{0T} \sin \epsilon}{(J_{0T} - J) \sin \beta_0 \cos^2 \beta_0 \cos(\beta_0 - \epsilon)} \right] E_T^{1/2} \quad (B17)$$

When advance ratio is zero, the advance ratio at zero thrust terms becomes unity in equations (B16) and (B17).

Generally steady-state propeller thrust coefficients are presented in propeller charts as a function of advance ratio, J . Then the linear with advance ratio thrust coefficient is obtainable as

$$C_T^* = -\left(\frac{\partial C_T}{\partial J}\right)_{J=J_{0T}} (J_{0T} - J) \quad (B18)$$

from which the derivatives with respect to β_0 or β can be evaluated. However, if only static conditions, $J=0$, data is available, then $\partial C_T / \partial J$ cannot be formulated. For this case the C_T^* derivatives can be obtained from equation (B10). The first and second derivatives of C_T^* in terms of C_T , are

$$\frac{C_T^{*'}}{C_T} = \left(\frac{C_T'}{C_T} + \frac{E_T'}{E_T}\right) E_T^{1/2} \quad (B19)$$

$$\frac{C_T^{*''}}{C_T} = \left[\frac{C_T''}{C_T} + \frac{E_T' C_T'}{E_T C_T} - \frac{1}{4} \left(\frac{E_T'}{E_T}\right)^2 + \frac{1}{2} \frac{E_T''}{E_T}\right] E_T^{1/2} \quad (B20)$$

where E_T is given in equation (B12), and the derivatives of E_T are, for $J = 0$

$$E_T' = \frac{75}{8} e_T^2 (\cos 2\beta_0 + \frac{3}{16} \sin 4\beta_0) \quad (B21)$$

$$E_T'' = \frac{75}{4} e_T^2 \left(\frac{3}{8} \cos 4\beta_0 - \sin 2\beta_0\right) \quad (B22)$$

Application of equations (B19) and (B20) provides approximate predictions of the linear with J thrust coefficient derivatives in terms of steady-state test or propeller theory thrust coefficient derivatives.

Power Coefficient Derivatives

The derivative ratios C_p' / C_p , and C_p'' / C_p are obtained by taking the derivatives of equation (B11) with respect to β_0 . The first and second derivatives divided by C_p are

$$\frac{C_p'}{C_p} = \frac{C_p^{*'}}{C_p^*} - \frac{1}{2} \frac{E_p'}{E_p} \quad (B23)$$

$$\frac{C_p''}{C_p} = \frac{C_p^{*''}}{C_p^*} - \frac{E_p'}{E_p} \frac{C_p^{*'}}{C_p^*} + \frac{3}{4} \left(\frac{E_p'}{E_p}\right)^2 - \frac{1}{2} \frac{E_p''}{E_p} \quad (B24)$$

where E_p is given in equation (B13), and the C_p^* and E_p derivatives are

$$\frac{C_p^{*'}}{C_p^*} = \frac{1}{\tan \beta_0} + \frac{J_{0P}'}{J_{0P} - J} \quad (B25)$$

$$\frac{C_p^{*''}}{C_p^*} = -1 + \frac{J_{0P}''}{J_{0P} - J} + \frac{2J_{0P}'}{(J_{0P} - J) \tan \beta_0} \quad (B26)$$

$$E_p' = 18 e_p^2 \frac{J}{J_{0P}} \left(1 - \frac{J}{J_{0P}}\right) \frac{J_{0P}'}{J_{0P}} \quad (B27)$$

$$E_p'' = 18 e_p^2 \frac{J}{J_{0P}} \left[\left(1 - \frac{J}{J_{0P}}\right) \frac{J_{0P}''}{J_{0P}} - \left(2 - 3 \frac{J}{J_{0P}}\right) \left(\frac{J_{0P}'}{J_{0P}}\right)^2 \right] \quad (B28)$$

where J_{0P} is given in equation (B7), and the derivatives are

$$J_{0P}' = \frac{2J_{0T}}{\sin 2\beta_0} + \frac{8d_0}{15} \left\{ \frac{21 \sin 6(\beta_0 - \beta_1)}{\sin \beta_0 \cos^3 \beta_0} - \frac{1 - 4 \sin^2 \beta_0}{\sin^2 \beta_0 \cos^4 \beta_0} [1 + 7 \sin^2 3(\beta_0 - \beta_1)] \right\} \quad (B29)$$

$$J_{0P}'' = \frac{2J_{0T}}{\cos^2 \beta_0} + \frac{16d_0}{15} \left\{ \frac{63 \cos 6(\beta_0 - \beta_1)}{\sin \beta_0 \cos^3 \beta_0} - \frac{21(1 - 4 \sin^2 \beta_0)}{\sin^2 \beta_0 \cos^4 \beta_0} \sin 6(\beta_0 - \beta_1) + \frac{1 - 3 \sin^2 \beta_0 + 8 \sin^4 \beta_0}{\sin^3 \beta_0 \cos^5 \beta_0} [1 + 7 \sin^2 3(\beta_0 - \beta_1)] \right\} \quad (B30)$$

At zero velocity, or in hover, the advance ratio is zero, then $E_p' = E_p'' = 0$, and the power coefficient derivatives greatly simplify. For $J = 0$

$$\frac{C_p'}{C_p} = \frac{1}{\tan \beta_0} + \frac{J_{0P}'}{J_{0P}} \quad (B31)$$

$$\frac{C_p''}{C_p} = -1 + \frac{2J_{0P}'}{J_{0P} \tan \beta_0} + \frac{J_{0P}''}{J_{0P}} \quad (B32)$$

REFERENCES

1. de Decker, R. W.: Investigation of an Isolated Monocyclic V/STOL Propeller Performance and Oscillatory Stress. USA AVLABS Technical Report 65-80, February 1966.
2. DeYoung, John: Cyclic-Control Propeller Theory. Vought Aeronautics Division Report No. 2-53340/9R-50577, June 1969.
3. Wadia, Aspi R.; and Fairchild, Jack E.: A Pure Direct Force/Moment Control for Coaxial Counterrotating Rotors. Paper presented at the Sixth North Texas Mini-Symposium Jointly sponsored by the AIAA and the University of Texas at Arlington, February 25, 1978.
4. DeYoung, John: Propeller at High Incidence. Journal of Aircraft, Vol. 2 No. 3, May-June 1965, pp. 241-250.
5. Ribner, H. S.: Propeller in Yaw. NACA Report 820, 1943. (See also NACA Report 819).
6. Gradshteyn, I. S.; and Ryzhik, I. M.: Table of Integrals, Series, and Products. Academic Press, Inc., New York and London, 1965, p. 952.
7. Glauert, Hermann: Airplane Propellers, Vol. IV, Division L of Aerodynamic Theory, W. F. Durand, ed. First Dover edition, Dover Publications, Inc., New York, 1963, p. 265.
8. Gessow, Alfred; and Myers, Jr., Garry C.: Aerodynamics of the Helicopter. The MacMillan Company, New York, 1952, p. 73.
9. Fung, Y. C.: The Theory of Aeroelasticity. John Wiley & Sons, Inc., New York, 1955, p. 323.

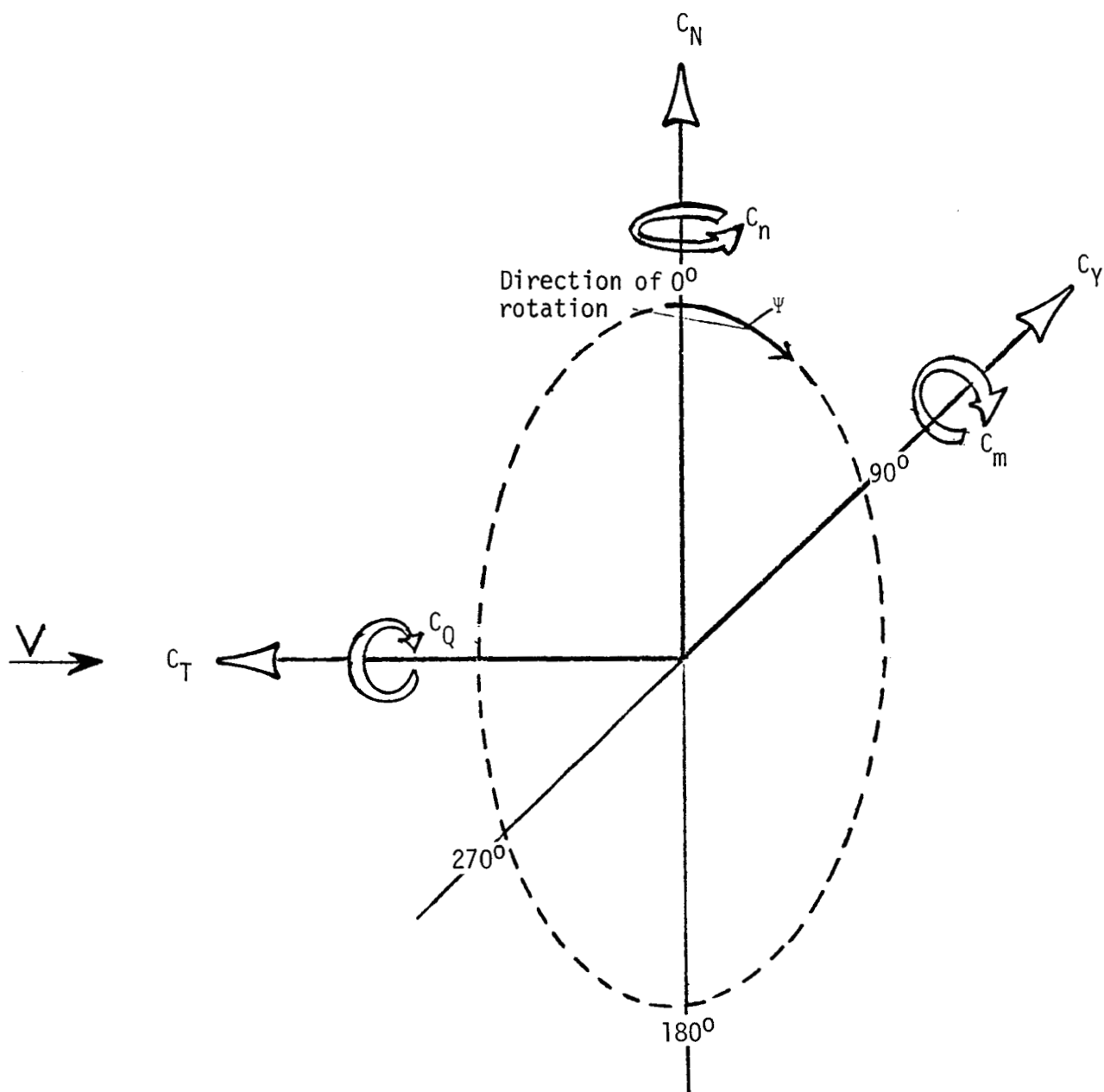


Figure 1. - Positive directions of propeller forces and moments.

1. Report No. NASA CR-3212	2. Government Accession No.	3. Recipient's Catalog No.	
4. Title and Subtitle Aircraft Control by Propeller Cyclic Blades		5. Report Date November 1979	6. Performing Organization Code
		8. Performing Organization Report No.	
7. Author(s) John DeYoung		10. Work Unit No.	
9. Performing Organization Name and Address Kentron International, Inc. Hampton Technical Center an LTV company 3221 N. Armistead Avenue, Hampton, VA 23666		11. Contract or Grant No. NAS1-13500	
		13. Type of Report and Period Covered Contractor Report	
12. Sponsoring Agency Name and Address National Aeronautics and Space Administration Washington, DC		14. Army Project No.	
15. Supplementary Notes Langley Technical Monitor: Harry H. Heyson Topical Report			
16. Abstract A theory is developed for aircraft control obtained from the propeller forces and moments generated by blade angle variation during a blade revolution. The propeller blade is pitched harmonically one cycle per propeller revolution which results in vehicle control forces and moments, termed cyclic-control. Using a power series representation of an arbitrary function of cyclic-blade angle, cyclic-control theory is developed which leads to exact solutions in terms of derivatives of steady-state thrust and power with respect to blade angle. An alternative solution, when the cyclic-blade angle function is limited to a sinusoidal cycle, is in terms of Bessel functions. An estimate of non-steady azimuth angle change or lag is presented. Cyclic-control analysis applied to the counter-rotating propeller shows that control forces or moments can be uniquely isolated from each other. Thus the dual rotor, in hovering mode, has propulsion without rotor tilt or moments, or, when in propeller mode at the tail of an airship or submarine, vehicle control with no vehicle movement. Control isolation is also attainable from three or more propellers in-line.			
17. Key Words (Suggested by Author(s)) Aircraft Control from Propulsion System Cyclic-Control Theory Propeller Forces and Moments Counterrotating Propeller Unique Control		18. Distribution Statement Unlimited - Unclassified Subject Category 02	
19. Security Classif. (of this report) Unclassified	20. Security Classif. (of this page) Unclassified	21. No. of Pages 59	22. Price* \$5.25